Inorg. Chem. **2008**, *47*, 4060−4076

Ligand Structure, Conformational Dynamics, and Excited-State Electron Delocalization for Control of Photoinduced Electron Transfer Rates in Synthetic Donor-Bridge-Acceptor Systems

Heather A. Meylemans, Chi-Fong Lei, and Niels H. Damrauer*

Department of Chemistry and Biochemistry, University of Colorado, Boulder, Colorado 80309

Received September 10, 2007

Synthesis, ground-, and excited-state properties are reported for two new electron donor-bridge-acceptor (D-B-A) molecules and two new photophysical model complexes. The D-B-A molecules are $[Ru(bpy)_2(bpy\text{-}\phi\text{-}MV)](PF_6)_4$ **(3)** and $[Ru(tmb)_2(bpy\text{-}\phi\text{-}MV)](PF_6)_4$ **(4)**, where bpy is 2,2′-bipyridine, tmb is 4,4′,5,5′-tetramethyl-2,2′-bipyridine, MV is methyl viologen, and ϕ is a phenylene spacer. Their model complexes are $[Ru(bpy)_2(p\text{-tol-bpy})](PF_6)_2$ **(1)** and $[Ru(tmb)_2(p\text{-tol-bpy})](PF_6)_2$ **(2)**, where *p*-tolyl-bpy is 4-(*p*-tolyl)-2,2′-bipyridine. Photophysical characterization of **1** and **2** indicates that 2.17 eV and 2.12 eV are stored in their respective ^{3}MLCT (metal-to-ligand charge transfer) excited state. These values along with electrochemical measurements show that photoinduced electron transfer ($D^*\text{-B-A} \rightarrow D^+\text{-B-A}^-$) is favorable in **3** and **4** with $\Delta G^\circ_{ET} = -0.52$ eV and -0.62 eV, respectively. The driving force for the reverse process ($D^+\text{-B-A}^- \rightarrow \text{D-B-A}$) is also reported: $\Delta G^\circ_{BET} = -1.7$ eV for **3** and -1.5 eV for **4**. Transient absorption (TA) spectra for **3** and **4** in 298 K acetonitrile provide evidence that reduced methyl viologen is observable at 50 ps following excitation. Detailed TA kinetics confirm this, and the data are fit to a model to determine both forward (k_{ET}) and back (k_{BET}) electron transfer rate constants: $k_{ET} = 2.6 \times 10^{10}$ s^{-1} for **3** and 2.8×10^{10} s^{-1} for **4**; $k_{BET} = 0.62 \times 10^{10}$ s^{-1} for **3** and 1.37×10^{10} s^{-1} for **4**. The similar rate constants k_{ET} for **3** and **4** despite a 100 meV driving force (ΔG°_{ET}) increase suggests that forward electron transfer in these molecules in room temperature acetonitrile is nearly barrierless as predicted by the Marcus theory. The reduction in electron transfer reorganization energy necessary for this barrierless reactivity is attributed to excited-state electron delocalization in the ^{3}MLCT excited states of **3** and **4**, an effect that is made possible by excited-state conformational changes in the aryl-substituted ligands of these complexes.

Introduction

Conversion of solar photons to electricity or fuels is a long-standing research goal in the chemical community.[1–18] It is also one that is being revisited with urgency as the risks of global climate change driven by society's reliance on carbonaceous energy resources is recognized and communicated.[16,19–21] In designing chemical systems to harvest solar photons, researchers have found inspiration in the mechanisms of photosynthetic organisms that rely on pho-

* To whom correspondence should be addressed. E-mail: niels.damrauer@colorado.edu.

(1) Nozik, A. J. *Annu. Rev. Phys. Chem.* **1978**, *29*, 189–222.
(2) Gray, H. B.; Maverick, A. W. *Science* **1981**, *214*, 1201–1205.
(3) Meyer, T. J. *Acc. Chem. Res.* **1989**, *22* (5), 163–170.
(4) O'Regan, B.; Gratzel, M. *Nature* **1991**, *353* (6346), 737–740.
(5) Wasielewski, M. R. *Chem. Rev.* **1992**, *92* (3), 435–461.
(6) Kalyanasundaram, K.; Gratzel, M. *Coord. Chem. Rev.* **1998**, *177*, 347–414.
(7) Gosztola, D.; Niemczyk, M. P.; Svec, W.; Lukas, A. S.; Wasielewski, M. R. *J. Phys. Chem. A* **2000**, *104* (28), 6545–6551.
(8) Gust, D.; Moore, T. A.; Moore, A. L. *Acc. Chem. Res.* **2001**, *34* (1), 40–48.
(9) Gratzel, M. *J. Photochem. Photobiol., C.* **2003**, *4* (2), 145–153.
(10) Nozik, A. J. *Inorg. Chem.* **2005**, *44* (20), 6893–6899.
(11) Wenger, O. S.; Leigh, B. S.; Villahermosa, R. M.; Gray, H. B.; Winkler, J. R. *Science* **2005**, *307* (5706), 99–102.
(12) Alstrum-Acevedo, J. H.; Brennaman, M. K.; Meyer, T. J. *Inorg. Chem.* **2005**, *44* (20), 6802–6827.
(13) Meyer, G. J. *Inorg. Chem.* **2005**, *44* (20), 6852–6864.
(14) Dempsey, J. L.; Esswein, A. J.; Manke, D. R.; Rosenthal, J.; Soper, J. D.; Nocera, D. G. *Inorg. Chem.* **2005**, *44* (20), 6879–6892.
(15) Wasielewski, M. R. *J. Org. Chem.* **2006**, *71* (14), 5051–5066.
(16) Lewis, N. S.; Nocera, D. G. *Proc. Natl. Acad. Sci. U.S.A.* **2006**, *103* (43), 15729–15735.
(17) Crabtree, G. W.; Lewis, N. S. *Physics Today* **2007**, *60* (3), 37–42.
(18) Kamat, P. V. *J. Phys. Chem. C* **2007**, *111* (7), 2834–2860.
(19) *Climate Change 2007: Impacts, Adaptation and Vulnerability*; IPCC Fourth Assessment Report, Climate Change 2007; Cambridge University Press: Cambridge, 2007.

10.1021/ic701776k CCC: $40.75
Published on Web 04/12/2008

toinduced electron transfer events to capture and convert energy. Plant photosynthesis utilizes the excited-state of the primary P680 chromophore within the reaction center of the membrane protein Photosystem II (PSII) to initiate a cascade of electron transfer and proton-coupled electron transfer events. These ultimately lead to multi-electron water oxidation, proton pumping, and the production of reductive equivalents to be used in the multi-electron carbon fixation chemistry initiated by Photosystem I (PSI) and its primary chromophore P700. Biomimetic approaches often focus on controlling initial events, namely long-distance photoinduced electron transfer, as a means of coupling light absorption with the production of redox equivalents for subsequent chemistry.[5,15,22–48] A key element to research of this type lies in manipulating structural features of synthetic systems in efforts to reduce rates of energy-wasting back electron transfer.

Despite their inspirational complexity[49–51] and efficiency with respect to charge separation, photosynthetic organisms are in general inefficient with respect to storage of solar energy in chemical fuels. Much of this stems from a substantial drop in stored redox potential with each electron or hole transfer event of the energy conversion mechanism. In PSII, the primary excited-state chromophore P680* contains 1.82 eV of energy, part of which will drive reactions related to water oxidation chemistry and part of which will be used towards reduction of the primary chromophore P700 photoexcited in PSI. By the time the nascent hole at P700 of PSI is reduced, more than 1 eV or 55% of the captured 1.82 eV of energy has been lost to heat. When one factors higher energy visible photons converted via energy transfer mechanisms to produce P680* in the first place, losses are far worse. Certainly energy wasting mechanisms evolved to reduce charge recombination rates, and within the photosynthetic reaction center of PSII, highly exergonic electron transfer events move the initial reduction equivalent of P680* by ∼28 Å in 200 ps, corresponding to a 34% drop in energy.[52,53]

We have been interested in designing chromophores that can produce and store charge-separated redox equivalents without relying on large negative ΔG and large distances for electron transfer as is done in natural systems. Specifically, we have been exploring whether systems can be engineered and synthesized to exploit conformationally active structural elements designed into the bridge of Donor-Bridge-Acceptor (D-B-A) systems as a strategy for trapping charge-separated redox equivalents. Our basic idea in this context is outlined in Scheme 1.

In step (i), MLCT (metal-to-ligand charge transfer) photoexcitation of a D-B-A system transfers charge from the metal center into the π^* system of the aryl-substituted ligand. Electronic and structural features of the molecule then evolve in time (step (ii)) as delocalization dynamics unfold concomitant with ring rotation. Our interest in ring-rotational motions is based on photophysical and ultrafast explorations by McCusker's group on Ru(II) MLCT systems containing aryl-substituted bipyridyl ligands (4,4′-diaryl-2,2′-bipyri-

(20) Hoffert, M. I.; Caldeira, K.; Jain, A. K.; Haites, E. F.; Harvey, L. D. D.; Potter, S. D.; Schlesinger, M. E.; Schneider, S. H.; Watts, R. G.; Wigley, T. M. L.; Wuebbles, D. J. *Nature* **1998**, *395* (6705), 881–884.

(21) *Basic Research Needs for Solar Energy Utilization*; Office of Science, U.S. Department of Energy: Washington, DC, 2005.

(22) Balch, A. L.; Olmstead, M. M. *Chem. Rev.* **1998**, *98* (6), 2123–2165.

(23) Barbara, P. F.; Meyer, T. J.; Ratner, M. A. *J. Phys. Chem.* **1996**, *100* (31), 13148–13168.

(24) Benniston, A. C.; Harriman, A. *Chem. Soc. Rev.* **2006**, *35* (2), 169–179.

(25) Berg, K. E.; Tran, A.; Raymond, M. K.; Abrahamsson, M.; Wolny, J.; Redon, S.; Andersson, M.; Sun, L. C.; Styring, S.; Hammarstrom, L.; Toftlund, H.; Akermark, B. *Eur. J. Inorg. Chem.* **2001**, (4), 1019–1029.

(26) Borgstrom, M.; Johansson, O.; Lomoth, R.; Baudin, H. B.; Wallin, S.; Sun, L. C.; Akermark, B.; Hammarstrom, L. *Inorg. Chem.* **2003**, *42* (17), 5173–5184.

(27) Borgstrom, M.; Shaikh, N.; Johansson, O.; Anderlund, M. F.; Styring, S.; Akermark, B.; Magnuson, A.; Hammarstrom, L. *J. Am. Chem. Soc.* **2005**, *127* (49), 17504–17515.

(28) Collin, J. P.; Guillerez, S.; Sauvage, J. P.; Barigelletti, F.; Decola, L.; Flamigni, L.; Balzani, V. *Inorg. Chem.* **1991**, *30* (22), 4230–4238.

(29) Cukier, R. I.; Nocera, D. G. *Annu. Rev. Phys. Chem.* **1998**, *49*, 337–369.

(30) Damrauer, N. H.; Hodgkiss, J. M.; Rosenthal, J.; Nocera, D. G. *J. Phys. Chem. B* **2004**, *108* (20), 6315–6321.

(31) Davis, W. B.; Svec, W. A.; Ratner, M. A.; Wasielewski, M. R. *Nature* **1998**, *396* (6706), 60–63.

(32) Davis, W. B.; Ratner, M. A.; Wasielewski, M. R. *J. Am. Chem. Soc.* **2001**, *123* (32), 7877–7886.

(33) Heimer, T. A.; Heilweil, E. J.; Bignozzi, C. A.; Meyer, G. J. *J. Phys. Chem. A* **2000**, *104* (18), 4256–4262.

(34) Imahori, H.; Guldi, D. M.; Tamaki, K.; Yoshida, Y.; Luo, C.; Sakata, Y.; Fukuzumi, S. *J. Am. Chem. Soc.* **2001**, *123* (27), 6617–6628.

(35) Imahori, H.; Tkachenko, N. V.; Vehmanen, V.; Tamaki, K.; Lemmetyinen, H.; Sakata, Y.; Fukuzumi, S. *J. Phys. Chem. A* **2001**, *105* (10), 1750–1756.

(36) Laine, P. P.; Bedioui, F.; Loiseau, F.; Chiorboli, C.; Campagna, S. *J. Am. Chem. Soc.* **2006**, *128* (23), 7510–7521.

(37) Macqueen, D. B.; Schanze, K. S. *J. Am. Chem. Soc.* **1991**, *113* (20), 7470–7479.

(38) Magnuson, A.; Frapart, Y.; Abrahamsson, M.; Horner, O.; Akermark, B.; Sun, L.; Girerd, J. J.; Hammarstrom, L.; Styring, S. *J. Am. Chem. Soc.* **1999**, *121* (1), 89–96.

(39) Newton, M. D. *Chem. Rev.* **1991**, *91* (5), 767–792.

(40) Oevering, H.; Paddonrow, M. N.; Heppener, M.; Oliver, A. M.; Cotsaris, E.; Verhoeven, J. W.; Hush, N. S. *J. Am. Chem. Soc.* **1987**, *109* (11), 3258–3269.

(41) Opperman, K. A.; Mecklenburg, S. L.; Meyer, T. J. *Inorg. Chem.* **1994**, *33* (23), 5295–5301.

(42) Osuka, A.; Marumo, S.; Mataga, N.; Taniguchi, S.; Okada, T.; Yamazaki, I.; Nishimura, Y.; Ohno, T.; Nozaki, K. *J. Am. Chem. Soc.* **1996**, *118* (1), 155–168.

(43) Rubtsov, I. V.; Susumu, K.; Rubtsov, G. I.; Therien, M. J. *J. Am. Chem. Soc.* **2003**, *125* (9), 2687–2696.

(44) Sauvage, J. P.; Collin, J. P.; Chambron, J. C.; Guillerez, S.; Coudret, C.; Balzani, V.; Barigelletti, F.; Decola, L.; Flamigni, L. *Chem. Rev.* **1994**, *94* (4), 993–1019.

(45) Watson, D. F.; Meyer, G. J. *Annu. Rev. Phys. Chem.* **2005**, *56*, 119–156.

(46) Weber, J. M.; Rawls, M. T.; MacKenzie, V. J.; Limoges, B. R.; Elliott, C. M. *J. Am. Chem. Soc.* **2007**, *129* (2), 313–320.

(47) Weller, A. *Z. Phys. Chem.* **1982**, *133* (1), 93–98.

(48) Yonemoto, E. H.; Riley, R. L.; Kim, Y. I.; Atherton, S. J.; Schmehl, R. H.; Mallouk, T. E. *J. Am. Chem. Soc.* **1992**, *114*, 8081–8087.

(49) Jordan, P.; Fromme, P.; Witt, H. T.; Klukas, O.; Saenger, W.; Krauss, N. *Nature* **2001**, *411* (6840), 909–917.

(50) Zouni, A.; Witt, H. T.; Kern, J.; Fromme, P.; Krauss, N.; Saenger, W.; Orth, P. *Nature* **2001**, *409* (6821), 739–743.

(51) Ferreira, K. N.; Iverson, T. M.; Maghlaoui, K.; Barber, J.; Iwata, S. *Science* **2004**, *303* (5665), 1831–1838.

(52) Moser, C. C.; Page, C. C.; Dutton, P. L. *Photochem. Photobiol. Sci.* **2005**, *4* (12), 933–939.

(53) Deisenhofer, J.; Norris, J. R., *The Photosynthetic Reaction Center*; Academic Press: San Diego, 1993; Vol. *1*.

Scheme 1. Design Scheme for Conformational Trapping of Charge-Separated Equivalents

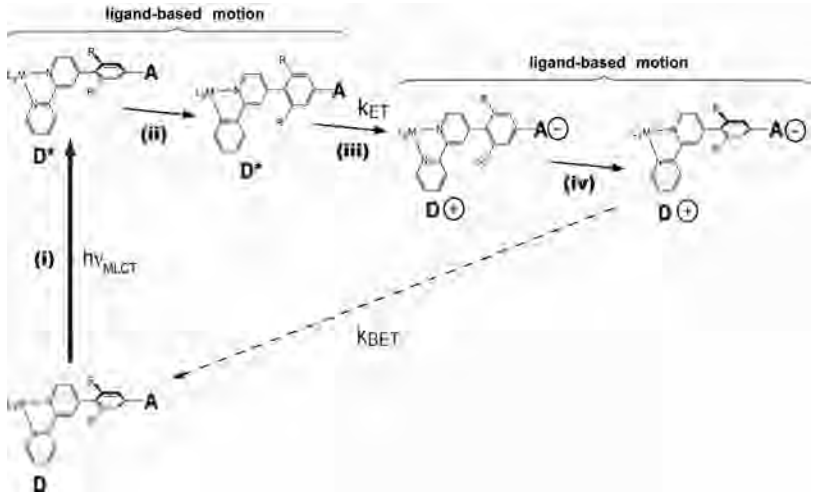

dine).[54–58] Theoretical[55,59] and structural evidence[54,55] suggests that steric interactions between the aryl-substituent (even for a sterically-unencumbered phenyl group) and protons of the bipyridine (bpy) ring system to which it is attached cause a non-coplanar aryl-bpy inter-ring geometry in the ground state of the metal complexes in much the same way that neutral biphenyl in the gas or solution phase is non-coplanar.[60–62] Upon MLCT photoexcitation of these complexes in solution with ultrashort visible laser pulses, dynamics are observed that have been attributed to ring-rotational motions occurring as the systems lower their energy within the excited-state manifold by maximizing the delocalization of the charge-transferred electron.[56,58] Such dynamics have been observed in $[Ru(dpb)_3]^{2+}$ (where, dpb = 4,4′-diphenyl-2,2′-bipyridine) on a ∼1 ps time scale in 298 K acetonitrile solution and are believed to occur after ^{1}MLCT → ^{3}MLCT intersystem crossing (∼100 fs).[63–67] In the context of Scheme 1, such motions are expected to alter key elements central to Marcus theory controlling rates of electron transfer to the acceptor (A). Certainly the electronic coupling H_{ab} between D*-B-A and D^+-B-A^- is expected to change as the π^*-system of the bridge evolves in time concomitant with interring torsional motions.[24,32] The superexchange pathway governing H_{ab} will be altered as orbital overlap and orbital energies within the bridge change during the excited-state delocalization phenomenon. Additionally, the inner-sphere reorganization energy λ_i as it pertains to C−C, C−N, and ring-breathing modes in the bridging ligand will be mitigated. Finally, the outer sphere reorganization energy λ_o will also decrease as the size of the electron donor increases and the distance of the electron transfer event shortens concomitant with excited-state electron delocalization on the bridge ligand. All of these processes should contribute to faster forward electron transfer rates. Once electron transfer to the methyl viologen acceptor is complete (step (iii)), electron-delocalization within the aryl-substituted ligand of the metal complex is irrelevant, and the inter-ring steric interactions in the bridge ligand are expected to force a non-coplanar geometry comparable to that of the ground state of the complex (step (iv)). We hypothesize that this reverse ring-rotation motion will inhibit back electron transfer to the hole at the metal center primarily by turning down the electronic coupling H_{ab} for this event. The combination of forward and reverse ring rotation motions would manage a type of "diode" favoring charge-separating photoreactions while inhibiting energy-wasting charge-recombination reactions. Certainly this control motif will be system dependent and highly regulated by the electronic structure of the D, B, and A moieties involved. For example, both Therien and co-workers[68] and Bocian and co-workers[69] have observed larger back electron transfer rates upon introduction of a phenylene spacer in comparison to systems without such a bridge.

The themes explored in Scheme 1, conformational tuning of bridge geometries and H_{ab} as well as the role of large amplitude molecular motions in governing electron transfer rates, are issues at the forefront of electron transfer re-

(54) Damrauer, N. H.; Boussie, T. R.; Devenney, M.; McCusker, J. K. *J. Am. Chem. Soc.* **1997**, *119* (35), 8253–8268.
(55) Damrauer, N. H.; Weldon, B. T.; McCusker, J. K. *J. Phys. Chem. A* **1998**, *102* (19), 3382–3397.
(56) Damrauer, N. H.; McCusker, J. K. *J. Phys. Chem. A* **1999**, *103* (42), 8440–8446.
(57) Damrauer, N. H.; McCusker, J. K. *Inorg. Chem.* **1999**, *38* (19), 4268–4277.
(58) Damrauer, N. H.; Curtright, A. E.; McCusker, J. K., manuscript in preparation.
(59) Lyubimova, O. O.; Baranovskii, V. I. *Zh. Strukt. Khim.* **2003**, *44* (5), 728–735.
(60) Almenningen, A.; Bastiansen, O.; Fernholt, L.; Cyvin, B. N.; Cyvin, S. J.; Samdal, S. *J. Mol. Struct.* **1985**, *128*, 59–76.
(61) Brock, C. P.; Minton, R. P. *J. Am. Chem. Soc.* **1989**, *111* (13), 4586–4593.
(62) Rubio, M.; Merchan, M.; Orti, E. *Theor. Chim. Acta* **1995**, *91* (1−2), 17–29.
(63) Damrauer, N. H.; Cerullo, G.; Yeh, A.; Boussie, T. R.; Shank, C. V.; McCusker, J. K. *Science* **1997**, *275* (5296), 54–57.
(64) McCusker, J. K. *Acc. Chem. Res.* **2003**, *36* (12), 876–887.
(65) Yeh, A.; Shank, C. V.; McCusker, J. K. *Science* **2000**, *289*, 935–938.
(66) Bhasikuttan, A. C.; Suzuki, M.; Nakashima, S.; Okada, T. *J. Am. Chem. Soc.* **2002**, *124* (28), 8398–8405.
(67) Yoon, S.; Kukura, P.; Stuart, C. M.; Mathies, R. A. *Mol. Phys.* **2006**, *104* (8), 1275–1282.
(68) Rubtsov, I. V.; Redmore, N. P.; Hochstrasser, R. M.; Therien, M. J. *J. Am. Chem. Soc.* **2004**, *126* (9), 2684–2685.
(69) Seth, J.; Palaniappan, V.; Wagner, R. W.; Johnson, T. E.; Lindsey, J. S.; Bocian, D. F. *J. Am. Chem. Soc.* **1996**, *118* (45), 11194–11207.

search.[24,32,36,46,68,70–73] Benniston and Harriman have recently reviewed how inter-component conformation can serve as a handle for tuning electron and energy transfer dynamics.[24] In their own work they have systematically altered the inter-ring dihedral angle of a biphenyl bridge moiety thereby showing which conformation favors electronic communication between two polypyridyl metal complex centers involved in a Dexter energy transfer mechanism. Bridge conformational dynamics are also very important. Lainé, Campagna, and co-workers have recently shown the importance of conformational locking to achieve "geometrical decoupling" of electroactive units in a D-B-A system. When conformational flexibility is allowed, electron transfer can be gated by the ligand based motions.[36,74] Wasielewski, Ratner, and co-workers have also recently shown that inter-ring conformational dynamics between aromatic donors (or acceptors) and aromatic bridges leads to conformational gating of electron transfer during both superexchange as well as hopping mechanisms.[32] They warn that such dynamics must be accounted for in efforts to use poly-aromatics as molecular wires. It should also be noted that protein systems can utilize large amplitude motions to manage electron transfer reactions necessary for bioenergetic conversion at regions of the conformational space far from the equilibrium geometry.[75]

Towards this goal of exploiting light-induced molecular motions to control forward and reverse electron transfer rates, we have synthesized two new D-B-A systems with an excited-state conformationally active bridge along with two new D-B model complexes having no acceptor. This manuscript describes their synthesis as well as their photophysical, electrochemical, and spectroelectrochemical characterization. We then show that electron-transfer photoproducts are observable and measure forward and reverse electron transfer rates. The forward rates as a function of driving force suggest these systems operate with low reorganization energy, suggesting participation by the conformationally active bridge in controlling electron transfer photochemistry. Characterization of these species with a battery of experimental techniques, as well as theory, provides us a foundation upon which to exploit excited-state structural motions to control electron transfer photoreactivity.

Experimental Section

General Information. All reagents and materials from commercial sources were used as received. Solvents for synthesis were purchased from Sigma-Aldrich. Transient absorption kinetic measurements were made using acetonitrile obtained from Burdick & Jackson (Acetonitrile-UV grade) as well as from in-house distillation of solvent obtained from Sigma-Aldrich. All deuterated solvents were obtained from Cambridge Isotope Laboratories, Inc. The ligand 2,2′-bipyridine (bpy) was purchased from Aldrich Chemical Co. The ligands 4,4′,5,5′-tetramethyl-2,2′-bipyridine[76] (tmb), 4-*p*-tolyl-2,2′-bipyridine[25] (*p*-tol-bpy), 4-(4-bromomethylphenyl)-2,2′-bipyridine[25] (brtb), and (1-methyl-4,4′-bipyridinium)PF_6[48] were prepared according to previously published procedures. The parent complex $[Ru(bpy)_3]Cl_2$ was purchased from Strem Chemicals. A standard salt metathesis and workup using NH_4PF_6 was undertaken to obtain $[Ru(bpy)_3](PF_6)_2$. $[Ru(tmb)_3](PF_6)_2$ was prepared according to previously reported procedures.[77] ^{1}H and 2D-NMR spectra were recorded on Varian Inova 400 or 500 MHz spectrometers. In the discussion of the chemical shifts below, hydrogens on the pyridyl rings of the substituted bipyridine ligand are abbreviated as *p*-tol-pyridyl-H. Elemental analyses were obtained through M-H-W Laboratories in Phoenix, AZ.

4-(1-(1′-Methyl-4,4′-bipyridinediium-1-yl)-methylphenyl)-2,2′-bipyridine (bpy-ϕ-MV^{2+}). A 0.4 mmol quantity of brtb and 0.8 mmol of [1-methyl-4,4′-bipyridinium]PF_6 were refluxed in 18 ml of CH_3CN under N_2 for 75 h. The CH_3CN was then removed by rotary evaporation. The solid was dissolved in H_2O and filtered through a medium frit. A 5-fold excess of NH_4PF_6 was added to the filtrate, and the resulting precipitate was filtered through a medium frit and rinsed with water. Yield: 202 mg (96%). ^{1}H NMR (CD_3CN) δ: 4.430 (s, 3H, N-methyl-H), 5.957 (s, 2H, methylene-H), 7.731 (m, 3H, aryl-H, *p*-tol-pyridyl-H), 7.947 (dd, 1H, J = 1.8 Hz, 5.5 Hz, *p*-tol-pyridyl-H), 8.055 (d, 2H, J = 8.4 Hz, aryl-H), 8.251 (t, 1H, J = 1.6 Hz, 7.8 Hz, *p*-tol-pyridyl-H), 8.401 (d, 2H, J = 6.6 Hz, MV-pyridyl-H), 8.456 (d, 2H, J = 6.9 Hz, MV-pyridyl-H), 8.602 (d, 1H, J = 8.0 Hz, *p*-tol-pyridyl-H), 8.762 (s, 1H, *p*-tol-pyridyl-H), 8.808 (d, 1H, J = 5.1 Hz, *p*-tol-pyridyl-H), 8.847 (d, 1H, J = 5.4 Hz, *p*-tol-pyridyl-H), 8.880 (d, 2H, J = 6.8 Hz, MV-pyridyl-H), 9.059 (d, 2H, J = 7.0 Hz, MV-pyridyl-H).

$[Ru(L)_2(p\text{-tol-bpy})](PF_6)_2$. The bis-heteroleptic ruthenium complexes **1** and **2** were prepared from a $[Ru(L)_2Cl_2]Cl\cdot 2H_2O$ precursor synthesized using a ruthenium blue starting material and the ligands L = bpy or tmb as previously reported.[78] This intermediate was then used directly for complexes **1** and **2** by refluxing with 1.5 equiv of *p*-tol-bpy ligand in EtOH for 8 h under N_2. Following reflux, the EtOH was removed by rotary evaporation. The residue was purified by column chromatography on silica with 5:4:1 CH_3CN/H_2O/sat. KNO_3 yielding the Ru complex as the nitrate salt. The solution was concentrated, and a 10-fold excess of NH_4PF_6 was then added; the precipitate was collected in a medium frit and washed with water.

(1) $[Ru(bpy)_2(p\text{-tol-bpy})](PF_6)_2$. Yield: 462 mg (94%) ^{1}H NMR (CD_3CN) δ: 3.35 (s, 3H, methyl-H), 7.43 (d, 1H, J = 8.3 Hz, *p*-tol-pyridyl-H), 7.55 (m, 5H, bpy-H), 7.68 (d, 2H, J = 6.0 Hz, aryl-H), 7.75 (m, 4H, bpy-H), 7.86 (d, 2H, J = 6.0 Hz, aryl-H), 7.87 (m, 1H, *p*-tol-pyridyl-H), 7.98 (d, 1H, J = 8.3 Hz, *p*-tol-pyridyl-H), 8.19 (m, 5H, bpy-H), 8.86 (m, 4H, bpy-H), 9.14 (s, 1H, *p*-tol-pyridyl-H), 9.16 (d, 1H, J = 8.0 Hz, *p*-tol-pyridyl-H) Anal. Calcd (found): C 46.79 (46.86), H 3.19 (3.31), N 8.87 (9.00).

(2) $[Ru(tmb)_2(p\text{-tol-bpy})](PF_6)_2$. Yield: 396 mg (87%) ^{1}H NMR (CD_3CN) δ: 2.102 (s, 12H, tmb-H), 2.437 (s, 12H, tmb-H), 3.351 (s, 3H, methyl-H), 7.301 (d, 2H, J = 5.5 Hz, aryl-H), 7.327 (s, 2H, tmb-H), 7.351 (s, 2H, tmb-H), 7.412 (s, 1H, *p*-tol-pyridyl-H),

(70) Helms, A.; Heiler, D.; McLendon, G. *J. Am. Chem. Soc.* **1991**, *113* (11), 4325–4327.
(71) Helms, A.; Heiler, D.; McLendon, G. *J. Am. Chem. Soc.* **1992**, *114* (15), 6227–6238.
(72) Holman, M. W.; Yan, P.; Ching, K. C.; Liu, R. C.; Ishak, F. I.; Adams, D. M. *Chem. Phys. Lett.* **2005**, *413* (4−6), 501–505.
(73) Yan, P.; Holman, M. W.; Robustelli, P.; Chowdhury, A.; Ishak, F. I.; Adams, D. M. *J. Phys. Chem. B* **2005**, *109* (1), 130–137.
(74) Ciofini, I.; Laine, P. P.; Bedioui, F.; Adamo, C. *J. Am. Chem. Soc.* **2004**, *126* (34), 10763–10777.
(75) Balabin, I. A.; Onuchic, J. N. *Science* **2000**, *290* (5489), 114–117.
(76) Mines, G. A.; Bjerrum, M. J.; Hill, M. G.; Casimiro, D. R.; Chang, I. J.; Winkler, J. R.; Gray, H. B. *J. Am. Chem. Soc.* **1996**, *118* (8), 1961–1965.
(77) Mabrouk, P. A.; Wrighton, M. S. *Inorg. Chem.* **1986**, *25* (4), 526–531.
(78) Togano, T.; Nagao, N.; Tsuchida, M.; Kumakura, H.; Hisamatsu, K.; Howell, F. S.; Mukaida, M. *Inorg. Chim. Acta* **1992**, *195* (2), 221–225.

7.425 (d, 1H, $J = 3.4$ Hz, *p*-tol-pyridyl-H), 7.530 (t, 1H, $J = 6.9$ Hz, *p*-tol-pyridyl-H), 7.666 (d, 1H, $J = 6.0$ Hz, *p*-tol-pyridyl-H), 7.733 (d, 2H, $J = 5.5$ Hz, aryl-H), 7.841 (d, 1H, $J = 6.0$ Hz, *p*-tol-pyridyl-H), 7.976 (d, 1H, $J = 8.1$ Hz, *p*-tol-pyridyl-H), 8.166 (t, 1H, $J = 8.0$ Hz, *p*-tol-pyridyl-H), 8.569 (s, 4H, tmb-H) Anal. Calcd (found): C 50.90 (50.30), H 4.37 (5.16), N 7.91, (7.88).

$[Ru(L)_2(bpy\text{-}\phi\text{-}MV)](PF_6)_4$. The bis-heteroleptic ruthenium complexes containing an electroactive ligand were prepared using a modified procedure to that described above. The $[Ru(L)_2Cl_2]Cl$ was first converted to $Ru(L)_2CO_3$ as previously described.[79] This complex was then reacted with 1.5 equiv of bpy-ϕ-MV^{2+} in 50:50 H_2O/EtOH saturated with KNO_3. This mixture was stirred at room temperature for 5 days in the dark. After 5 days, the solvent was removed by rotary evaporation. The residue was purified by column chromatography on silica with 5:4:1 CH_3CN/H_2O/sat. KNO_3 yielding the Ru complex as the nitrate salt. The solution was concentrated, and a 10-fold excess of NH_4PF_6 was then added; the precipitate was collected in a medium frit and washed with water.

(3) $[Ru(bpy)_2(bpy\text{-}\phi\text{-}MV)](PF_6)_4$. Yield: 155.5 mg (83%) ^{1}H NMR (CD_3CN) δ: 4.430 (s, 3H, N-methyl-H), 5.938 (s, 2H, methylene-H), 7.448 (m, 5H, bpy-pyridyl-H), 7.671(dd, 1H, $J = 2$ Hz, 6.2 Hz, *p*-tol-pyridyl-H), 7.693 (d, 2H, $J = 8.4$ Hz, aryl-H), 7.788 (m, 5H, bpy-H), 8.008 (d, 2H, $J = 8.4$ Hz, aryl-H), 8.102 (m, 5H, bpy-H), 8.400 (d, 2H, $J = 6.5$ Hz, MV-pyridyl-H), 8.458 (d, 2H, $J = 7.0$ Hz, MV-pyridyl-H), 8.541 (m, 5H, bpy-H), 8.708 (d, 1H, $J = 8.2$ Hz, *p*-tol-pyridyl-H), 8.762 (s, 1H, *p*-tol-pyridyl-H), 8.881 (d, 2H, $J = 6.6$ Hz, MV-pyridyl-H), 9.044 (d, 2H, $J = 7.0$ Hz, MV-pyridyl-H) Anal. Calcd (found): C 40.89 (40.58), H 2.86 (3.07), N 7.95 (7.97).

(4) $[Ru(tmb)_2(bpy\text{-}\phi\text{-}MV)](PF_6)_4$. Yield: 71.6 mg (68%) ^{1}H NMR (CD_3CN) δ= 2.09 (s, 12H, tmb-methyl-H), 2.43 (s, 12H, tmb-methyl-H), 4.40 (s, 3H, N-methyl-H), 5.92 (s, 2H, methylene-H), 7.33 (s, 4H, tmb-H), 7.37 (m, 1H, *p*-tol-pyridyl-H), 7.62 (dd, 1H, $J = 6.0$ Hz, 9.8 Hz, *p*-tol-pyridyl-H), 7.70 (d, 2H, $J = 8.1$ Hz, aryl-H), 7.74 (m, 2H, *p*-tol-pyridyl-H), 7.98 (d, 2H, $J = 8.1$ Hz, aryl-H), 8.03 (t, 1H, $J = 7.7$ Hz, *p*-tol-pyridyl-H), 8.24 (s, 4H, tmb-H), 8.39 (d, 2H, $J = 6.5$ Hz, MV-pyridyl-H), 8.44 (d, 2H, $J = 6.7$ Hz, MV-pyridyl-H), 8.69 (d, 1H, $J = 7.7$ Hz, *p*-tol-pyridyl-H), 8.71 (s, 1H, *p*-tol-pyridyl-H), 8.85 (d, 2H, $J = 6.5$ Hz, MV-pyridyl-H), 9.04 (d, 2H, $J = 6.7$ Hz, MV-pyridyl-H) Anal. Calcd (found): C 40.35 (40.54), H 3.39 (3.47), N 6.72 (6.68).

Physical Measurements. Cyclic Voltammetry. Electrochemical measurements were carried out with a BAS 100A electrochemical analyzer. Solutions of the compound were dissolved in anhydrous CH_3CN containing 0.1 M NH_4PF_6 as the supporting electrolyte. A standard three-electrode setup was used with a working Pt electrode, Pt wire counter electrode, and a $Ag/AgNO_3$ reference electrode. All measurements were made after an argon purge using ferrocene as an internal reference.[80]

Spectro-Electrochemistry. Measurements were taken using the BAS100A electrochemical analyzer held at constant voltage. Spectra were recorded with an Agilent 8453 UV-Vis spectrophotometer. The OTTLE cell (Optically Transparent Thin-Layer Electrode) used for these measurements was homebuilt with materials commercially available from BAS, Aldrich, and NSG Precision Cells, Inc. The transparent working electrode was a platinum mesh (Aldrich Platinum Gauze, Mesh 100) spot-welded to a platinum wire. The auxiliary electrode was platinum wire (Aldrich 0.25mm diameter). The reference electrode was made from the non-aqueous electrode kit available through BAS. The electrodes were placed in a modified 2 mm path length glass cell fitted with a lid to help maintain an oxygen-free environment. All measurements were made using a freshly prepared solution of 0.075 M NH_4PF_6 in anhydrous CH_3CN. The concentration of sample in this solution varied between 0.5 and 1.0 mM as needed to obtain good signal to noise with relevant peak absorbances less than 2. All samples were purged with argon before voltage was applied. Spectra were collected every 0.5−1 min for a total of 15 min.

Absorption and Emission Spectra. All spectroscopic data were obtained on samples dissolved in anhydrous CH_3CN. Absorption spectra were measured with a Hewlett-Packard HP8452A diode array UV-vis spectrophotometer. Emission spectra were collected for deoxygenated solutions of each complex having an optical density of about 0.1 (1 cm path length) at the excitation wavelength using a PTI QM-4 fluorometer. Samples were deoxygenated using a diffusion pump setup in which 5 freeze-pump-thaw cycles were performed on each sample. At the end of five cycles the pressure in the cell upon freezing was between 40−60 μTorr and did not change with continued pumping.

Background emission measurements on solvent blanks revealed no signals other than the expected Raman lines of the neat solvent. Excitation spectra in the region of the ^{1}MLCT ← GS visible absorption band ($\lambda > 400$ nm), corrected for the Xe lamp spectral profile, matched the ground-state absorption spectrum for each of the Ru complexes studied. Therefore, all spectral and quantum yield measurements were carried out at a single excitation wavelength of 450 nm near the MLCT maximum. The resolution of the spectrometer is estimated to be 2 nm based on the reciprocal linear dispersion of the emission monochromator and the slit setting of the instrument. Emission spectra were corrected for instrument response using a tungsten lamp provided by the manufacturer, which has been calibrated against a NIST standard tungsten lamp. All subsequent data manipulations were carried out using the corrected spectra.

Radiative quantum yield (Φ_r) measurements of new compounds were made relative to $[Ru(bpy)_3](PF_6)_2$ in 298 K CH_3CN ($\Phi_r = 0.062$)[81] on optically thin solutions (OD $\approx$ 0.1). Values are calculated according to the following equation,[82]

$$\Phi_{unk} = \Phi_{std}\left(\frac{I_{unk}}{A_{unk}}\right)\left(\frac{A_{std}}{I_{std}}\right)\left(\frac{\eta_{unk}}{\eta_{std}}\right)^2 \quad (1)$$

where Φ_{unk} is the radiative quantum yield of the sample, Φ_{std} is the radiative quantum yield of the $[Ru(bpy)_3](PF_6)_2$ standard, I_{unk} and I_{std} are integrated emission intensities of the sample and the standard, respectively, A_{unk} and A_{std} are the absorbances of the sample and the standard, respectively, at the excitation wavelength (450 nm), and η_{unk} and η_{std} are the indexes of refraction of the samples and standard solutions. Because both measurements were taken in the same solvent, the last term is 1.

The corrected emission spectra were converted from wavelength data into energy units, and the correction of Parker and Rees was applied.[83] Fitting of the spectra involved multiparameter least squares minimization of eq. 2 to the data. The best fit was determined both by visual inspection as well as minimization of the root-mean-squared deviation.[84–86]

(79) Sullivan, B. P.;Salmon, D. J.;Meyer, T. J. *Inorg. Chem.* **1978**, (*17*), 3334–3341.
(80) Gagne, R. R.; Koval, C. A.; Lisensky, G. C. *Inorg. Chem.* **1980**, *19* (9), 2854–2855.
(81) Calvert, J. M.; Caspar, J. V.; Binstead, R. A.; Westmoreland, T. D.; Meyer, T. J. *J. Am. Chem. Soc.* **1982**, *104* (24), 6620–6627.
(82) Demas, J. N.; Crosby, G. A. *J. Phys. Chem.* **1971**, *75* (8), 991–1024.
(83) Parker, C. A.; Rees, W. T. *Analyst (London)* **1960**, *85*, 587–600.
(84) Kober, E. M.; Caspar, J. V.; Lumpkin, R. S.; Meyer, T. J. *J. Phys. Chem.* **1986**, *90*, 3722–3734.

$$I(\bar{\nu}) = \sum_{\nu''=0}^{n} \left\{ \left(\frac{E_0 - \nu''\hbar\omega}{E_0} \right)^3 \left(\frac{S^{\nu''}}{\nu''!} \right) \times \exp\left[-4 \ln(2) \left(\frac{\bar{\nu} - E_0 + \nu''\hbar\omega}{\Delta\bar{\nu}_{0,1/2}} \right) \right]^2 \right\} \quad (2)$$

Details of the fitting parameters are discussed below in the results, but it is important to note that the value of $\hbar\omega$ was held constant in all fits at 1350 cm^{-1} as this is an over parameterized fit and the most important values for our query are those of E_0 and $\Delta\bar{\nu}_{0,1/2}$. The value of 1350 cm^{-1} is the reported value for $\hbar\omega$ for $Ru(bpy)_3^{2+}$ in low temperature studies, which should be similar to our complexes.[87] The Huang−Rhys factor S_M, also obtained in fitting to this equation, reflects the degree of vibronic coupling between the initial and final states involved in the emission process. A smaller value for S_M indicates decreased nuclear distortion of the excited state relative to the ground state along a "single" coordinate whose frequency is the same as that used in the specification of $\hbar\omega$.

Nanosecond Time-Resolved Emission. Time-resolved emission measurements were carried out using a spectrometer of local origin. A broadband laser pulse train (∼800 nm ± 17 nm; ∼50 fs temporal FWHM; 1 KHz; ∼900 mJ/pulse) is derived from a source consisting of a commercial Ti:Sapphire multi-pass amplifier (Quantronix; Odin) seeded by a commercial Ti:Sapphire oscillator (K&M Labs) as described elsewhere.[88] The amplified pulse train was attenuated to <25% of total power and transmitted through a 100 μm β-barium borate (BBO) crystal (Type I, 30°) to generate the second harmonic of the fundamental centered at 400 nm. The output was filtered to remove any unconverted fundamental and then loosely focused on a 298 K optically thin and thoroughly degassed (with 5 freeze-pump thaw cycles as described above) sample in acetonitrile (∼6 × 10^{-6} M; 1 cm path length). The emitted light was collected at 90° to the excitation via back-to-back plano-convex lenses (f_o = 25.4 mm; diameter = 25.4 mm), passed through a 10 nm bandpass filter (640 ± 5 nm; Thorlabs FB640-10), and detected using a PMT (Hamamatsu; H9305-02) negatively biased at −900 V. The time resolution of this detector is ∼1.4 ns. The PMT signal was terminated through a 50 Ω resistor to a LeCroy Model 9384L digitizing oscilloscope. Linearity of the PMT signal was checked, with the signal intensity adjusted if necessary via attenuation of the excitation beam using neutral density filters. A 5000-shot signal average was collected, transferred to a computer, and processed using programs of local origin.

Picosecond Transient Absorption Kinetics and Spectra. Transient absorption kinetics were acquired using a pump-probe spectrometer derived from the same amplified Ti:Sapphire laser system described above. For these measurements ∼700 mW of the amplified 1 KHz pulse train was coupled into an optical parametric amplifier (Light Conversion; Topas) to produce 480 ± 10 nm pulses with time resolution <100 fs/pulse. This 480 nm pulse train was passed through an optical chopper (ThorLabs MC1000) synchronized at ω/2 (500 Hz) with respect to the 1 KHz laser system, directed onto a computer controlled translation stage (Newport: 3.3 fs/step time resolution), and gently focused (using a 300 mm focal length lens) into a 2 mm path length optical cell containing the sample dissolved in acetonitrile with an optical density of ∼0.5 (∼2 × 10^{-5} M) at 480 nm. The pump polarization was horizontal at the sample and ∼2 μJ/pulse were used for excitation. The sample (∼1 mL) was continuously stirred using a small stir bar driven by a rotating magnet mounted at the face of the sample. This minimized the effect of thermal lensing due to the pump laser while allowing for small sample volumes. Sample degradation was not observed in the comparison between visible absorption spectra collected before and after the transient absorption measurements were made.

For much of the transient absorption data discussed, the probe pulses were derived from white-light continuum generated by focusing ∼1 μJ of the amplified pulse train into a 1 mm disk of CaF_2 (continuously moving side-to-side to prevent burning of the substrate). For those kinetics reported for **4** in Figure 5 (top and middle), as well as repeat measurements of kinetics at λ_{probe} = 607 nm for **3** and **4**, the probe pulses were derived from white-light continuum generated by focusing ∼1 μJ of the amplified pulse train into a 1 mm disk of sapphire. In both cases of white-light continuum generation (sapphire or CaF_2), an off-axis parabolic mirror was used to collimate the white light after its generation, and a spherical concave mirror with a focal length of 250 mm was used to focus it into the sample at an acute angle (<3°) with respect to the pump. After the sample, the broad-band probe was passed through a polarizer (transmitting horizontal polarization) and analyzed for single wavelength or spectral measurements.

For single wavelength kinetics measurements, the broad-band probe was coupled into a 300 mm scanning monochromator (Acton; Spectra Pro 2300i) set to the appropriate wavelength. A 1200 grooves/mm grating was used with 1 mm entrance and exit slits providing spectral resolution of 2.7 nm. An amplified Si photodiode (Thor labs; PDA-55) joined to the exit slit of the monochromator was used to collect the signal. This was then sent to a digital lockin amplifier (Stanford Research; SR810 DSP) synchronized to the chopper frequency. The lockin reports a change in transmittance as excited state absorption or bleach transitions are produced by the pump pulse. Kinetics traces were collected by monitoring this signal as a function of the position of the motorized translation stage, and the data are reported as a normalized change in transmittance ($-\Delta T$). The kinetics traces reported herein represent an average of 10 scans of positions in both the forward and the reverse directions of the translation stage. The data collection software was written in house (National Instruments, Labview 7.0). For fitting of these data to the kinetics model discussed herein, we used the commercially available data analysis software Igor Pro 4.0 (WaveMetrics).

Transient spectra were collected using a diode array spectrometer to monitor probe intensity as a function of wavelength at different arrival times of the white-light probe. For each time point, the white light spectrum was averaged for 25 milliseconds (Ocean Optics USB 2000 with 400 micrometer fiber), and ΔA (as a function of wavelength) was calculated using the spectral information from the first time point (negative time meaning the probe has arrived before the pump) to report the white-light spectrum through the sample in the absence of pump. Transient spectra reported herein represent the average of 720 scans. No effort was made to correct these for the temporal chirp of the probe pulses which is <1 ps over the spectral range that is available. The data were collected using Labview programs of local origin.

Results and Discussion

Synthetic Protocols. To begin exploring the role of excited-state ligand based motions in modulating photo-induced electron transfer rates we have synthesized two

(85) Claude, J. P. Photophysics of Polypyrodyl Complexes of Ruthenium (II), Osmium(II), and Rhenium(I). Ph.D. Thesis, University of North Carolina, Chapel Hill, NC, 1995.
(86) Claude, J. P.; Meyer, T. J. *J. Phys. Chem.* **1995**, *99* (1), 51–54.
(87) Caspar, J. V.; Meyer, T. J. *J. Am. Chem. Soc.* **1983**, *105*, 5583–5590.
(88) Montgomery, M. A.; Meglen, R. R.; Damrauer, N. H. *J. Phys. Chem. A* **2006**, *110*, 6391–6394.

Scheme 2. Ruthenium(II) Polypyridine Complexes **1**−**4**

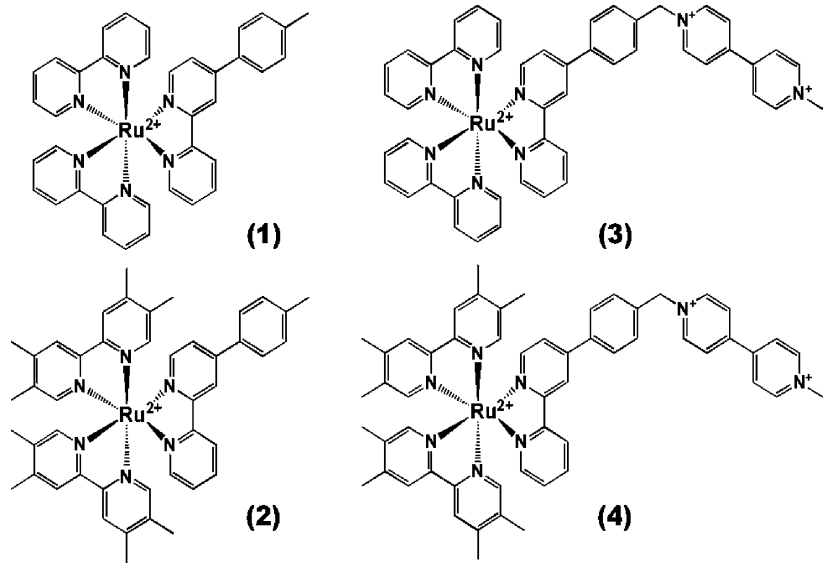

D-B-A systems described below that juxtapose a Ru(II) polypyridyl excited-state electron donor (D) with a methylviologen acceptor (A) through a bridge (B) that participates in inter-ring rotational motions. Photoinduced electron transfer systems utilizing a Ru(II) MLCT excited state as a donor and a covalently-bound methyl viologen or paraquat derivative as an acceptor have been demonstrated by other groups.[48,89–95] In fact, this D and A design motif has been a workhorse in the development of intramolecular electron transfer research. Electron transfer rates (forward and backward) have been reported for a number of these systems, and in cases where the bridge is sufficiently rigid to inhibit harpooning effects,[23] charge-separated intermediates have been directly observed using transient absorption techniques.[48,89,90,94]

The D-B-A systems we have designed and synthesized are shown in Scheme 2 as compounds **3** and **4**. The corresponding donor complexes **1** and **2** were also synthesized for control purposes as discussed throughout the manuscript. For each of these bis-heteroleptic complexes we have found it useful to isolate the Ru(III) species $[Ru(L)_2Cl_2]Cl$ following reaction of a "Ruthenium Blue" starting material with two equivalents of the ancillary ligand. In our hands this compound can be isolated with higher yield and purity than the $Ru(II)L_2Cl_2$ precursor frequently used for synthesis of bis-heteroleptic Ru(II) polypyridyl complexes.[96] This $[Ru(L)_2Cl_2]Cl$ species can then easily undergo reduction and chloride ligand exchange. For the donor complexes **1** and **2** it was possible to achieve this directly by refluxing $[Ru(L)_2Cl_2]Cl$ with 4-*p*-tolyl-2,2′-bipyridine in EtOH. Towards synthesis of the D-B-A systems **3** and **4**, we isolated a second precursor RuL_2CO_3 where the reduction step is completed prior to the addition of the electroactive bipyridine ligand. Further, the two chloride ligands have been replaced with a single doubly-charged anion. These characteristics allow for more facile ligand exchange under milder conditions with the positively charged acceptor ligand.

The asymmetric aryl-substituted ligand in each of these complexes has a common synthetic step involving the Krönhke condensation.[97] This methodology uses inexpensive starting materials and can be easily modified to append various substituents, both aryl and otherwise, to one of the pyridine rings of a polypyridyl system. Procedures of this nature have been shown to produce substituted bipyridyl and terpyridyl species.[25,44,98,99] All asymmetric ligands utilize this step with yields of 40−60%. Following this reaction, the diimine product was either used directly in the donor model complexes **1** and **2** or carried through to add the electroactive acceptor. The addition of the acceptor was achieved using radical bromination of the primary methyl group, followed by SN_2 addition of singly charged (1-methyl-4,4′-bipyridinium)PF_6. Salt metathesis using NH_4PF_6 completed the synthesis of the asymmetric doubly-charged electroactive ligand as a PF_6 salt. Each of the steps following the condensation resulted in yields >80% allowing for generation of the acceptor ligand with reasonable yield.

(89) Yonemoto, E. H.; Saupe, G. B.; Schmehl, R. H.; Hubig, S. M.; Riley, R. L.; Iverson, B. L.; Mallouk, T. E. *J. Am. Chem. Soc.* **1994**, *116*, 4786–4795.
(90) Lomoth, R.; Haupl, T.; Johansson, O.; Hammarstrom, L. *Chem.*−*Eur. J.* **2002**, *8* (1), 102–110.
(91) Elliott, C. M.; Freitag, R. A.; Blaney, D. D. *J. Am. Chem. Soc.* **1985**, *107* (16), 4647–4655.
(92) Cooley, L. F.; Headford, C. E. L.; Elliott, C. M.; Kelley, D. F. *J. Am. Chem. Soc.* **1988**, *110* (20), 6673–6682.
(93) Cooley, L. F.; Larson, S. L.; Elliott, C. M.; Kelley, D. F. *J. Phys. Chem.* **1991**, *95* (26), 10694–10700.
(94) Kelly, L. A.; Rodgers, M. A. J. *J. Phys. Chem.* **1995**, *99* (35), 13132–13140.
(95) BergBrennan, C.; Subramanian, P.; Absi, M.; Stern, C.; Hupp, J. T. *Inorg. Chem.* **1996**, *35* (12), 3719–3722.
(96) Sullivan, B. P.; Salmon, D. J.; Meyer, T. J. *Inorg. Chem.* **1978**, *17* (12), 3334–3341.
(97) Zecher, W.; Krohnke, F. *Chem. Ber. Recl.* **1961**, *94* (3), 690–697.
(98) Cordaro, J. G.; McCusker, J. K.; Bergman, R. G. *Chem. Commun.* **2002**, (14), 1496–1497.
(99) Johansson, O.; Borgstrom, M.; Lomoth, R.; Palmblad, M.; Bergquist, J.; Hammarstrom, L.; Sun, L. C.; Akermark, B. *Inorg. Chem.* **2003**, *42* (9), 2908–2918.

Table 1. Photophysical Properties of Complexes in Room Temperature CH_3CN

complex	$MLCT_{max}$/nm	$\varepsilon/M^{-1}\ cm^{-1}$	$\lambda_{em\ max}$/nm	ϕ_{em}[a]	$\tau_{obs} = 1/k_o/\mu s$	$k_r/10^5\ s^{-1}$	$k_{nr}/10^5\ s^{-1}$
$[Ru(bpy)_3](PF_6)_2$	452	13000[b]	615	0.062[b]	1.0	0.62	9.3
$[Ru(tmb)_3](PF_6)_2$	448	8100	600	0.044 ± 0.001	0.41	1.07	23.2
1	455	17450	623	0.08 ± 0.01	0.94	0.86	9.7
2	449	13730	650	0.040 ± 0.002	0.87	0.46	11.0
3	455	15360					
4	444	15110					

[a] Error bars represent reproducibility within 2σ for three separate measurements of each complex. [b] These data were taken from Juris et.al.[100]

All of the novel ruthenium complexes synthesized are asymmetric having C_1 symmetry. Microcrystalline materials have been isolated for each compound; however, numerous attempts to grow single crystals adequate for X-ray determination have been unsuccessful. To aid in the characterization of the complexes, various NMR techniques were utilized in addition to elemental analysis. All complexes were characterized using ^{1}HNMR and 2D COSY to assist in assigning protons in the aromatic region. Because of the complexity of the ^{1}HNMR for the D-B-A complexes **3** and **4**, HMBC and HSQC experiments were also undertaken so that carbon shifts could augment assignments made using 2D COSY. We have also undertaken NOESY and DOESY experiments for these complexes allowing us to verify that all of the peaks seen in the ^{1}HNMR spectrum belonged to a single compound rather than multiple compounds with similar features.

Photophysics. To estimate the driving force for photoinduced electron transfer it is important to measure the amount of energy stored (ΔG°_{MLCT}) in the ^{3}MLCT excited state of **3** and **4** prior to electron transfer. This quantity is related to the so-called E_0 discussed below. However, these compounds do not exhibit ^{3}MLCT $\rightarrow$ ^{1}GS emission, which precludes use of a Franck−Condon analysis to determine E_0.[84–86] Thus, it was important to synthesize complexes **1** and **2** as photophysical models for complexes **3** and **4**, respectively.

The photophysical properties of **1**−**4** were measured at room temperature in acetonitrile. A number of relevant ground and ^{3}MLCT state characteristics are listed in Table 1. Each of these compounds produces an absorption spectrum exhibiting an intense visible ^{1}MLCT $\leftarrow$ ^{1}GS band as the lowest energy electronic transition (see Figure 1 and Supporting Information, Figure S1). The absorption spectra for compounds **1**−**4** are comparable to their respective parent complexes $[Ru(bpy)_3](PF_6)_2$ and $[Ru(tmb)_3](PF_6)_2$. In complexes **1** and **3** there is near perfect overlap of the normalized absorption spectra (Figure 1) indicating that the MV^{2+} moiety does not perturb the MLCT absorption properties. Presumably this is a consequence of the CH_2 spacer, which has no energetically accessible π-system separating the donor and acceptor moieties.

The overlay of UV-vis absorption spectra for **2** and **4** is shown in the Supporting Information, Figure S1a and again there is good overlap between the MLCT features. Initially we observed a subtle difference between the two spectra (Supporting Information, Figure S1b) in the form of a shoulder at the red edge of the MLCT band. We believed this to be evidence of a small percentage of colored impurity which also manifests itself in the observation of a long-lived transient absorption kinetics feature. Upon further investigation, we have discovered that this shoulder is not observed when a sample of **3** is dissolved in CD_3CN (Cambridge Isotope Laboratories, Inc.) (Supporting Information, Figure S1c). It is significantly reduced when a sample of **3** is dissolved in CH_3CN obtained from a specialist retailer (Burdick & Jackson acetonitrile−UV grade) (Supporting Information, Figure S1a) rather than from our in-house solvent still that utilizes an anhydrous alumina column coupled to a commercial source of bulk CH_3CN (Aldrich Reagent Plus grade acetonitrile). We are currently investigating the nature of the impurity and why it forms from clean samples of **3** and **4** more readily with certain CH_3CN solvent batches.

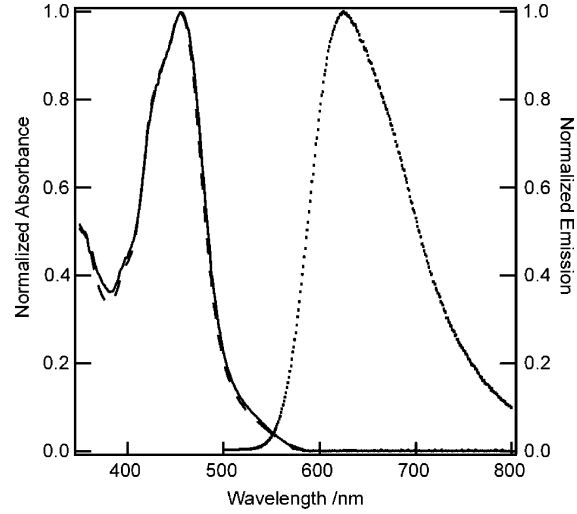

Figure 1. Normalized UV-vis absorption spectrum for **1** (dashed line) and **3** (solid line) in 298 K CH_3CN. The corrected emission spectrum of **1** collected in deoxygenated CH_3CN at 298 K is also shown (dotted line).

Electronic excitation of the model complexes **1** and **2** at 450 nm leads to the observation of a broad and featureless emission band as shown in Figure 1 and Supporting Information, Figure S1, respectively. These bear strong resemblance to the well known ^{3}MLCT $\rightarrow$ ^{1}GS characteristic of related Ru(II) polypyridyl systems[100] and certainly the parent complexes $[Ru(bpy)_3]^{2+}$ and $[Ru(tmb)_3]^{2+}$. Of note, the emission maximum for **2** is substantially red shifted with respect to its parent complex $[Ru(tmb)_3]^{2+}$, $[Ru(bpy)_3]^{2+}$, and **1**. Radiative quantum yields (ϕ_{em}) were also measured for these species and are listed in Table 1.

The D-B-A species **3** and **4** are non-emissive at room temperature, indicating that they possess one or more additional excited-state decay pathways beyond what is

(100) Juris, A.; Balzani, V.; Barigelletti, F.; Campagna, S.; Belser, P.; Von Zelewsky, A. *Coord. Chem. Rev.* **1988**, *84*, 85–277.

Table 2. Emission Spectral Fitting Data for Complexes in Room Temperature CH_3CN

complex	E_0/cm^{-1}	$\Delta G^\circ_{MLCT}/cm^{-1}$	$\hbar\omega_M/cm^{-1}$	S_M	$\Delta\bar{\nu}_{0,1/2}/cm^{-1}$
$[Ru(bpy)_3](PF_6)_2$	16310 ± 70	17630 ± 70	1350	0.98 ± 0.05	1740 ± 40
$[Ru(tmb)_3](PF_6)_2$	16580 ± 70	17810 ± 70	1350	0.97 ± 0.05	1680 ± 40
1	16190 ± 70	17490 ± 70	1350	0.92 ± 0.05	1730 ± 40
2	15550 ± 70	17120 ± 70	1350	0.85 ± 0.05	1900 ± 40

The error bars for the parameters reported in this table represent 2σ determined from five separate measurements and fittings of emission data collected for $[Ru(bpy)_2(p\text{-tolbpy})](PF_6)_2$ **1** in 298 K acetonitrile.

Table 3. Electrochemical Data in Room Temperature CH_3CN vs SCE

	$E_{1/2}$					
complex	$(Ru^{III/II})$/V	$MV^{2+/1+}$/V	$MV^{1+/0}$/V	1st ligand red./V	2nd ligand red./V	$\Delta E_{(redox)}$/V
$[Ru(bpy)_3](PF_6)_2$	1.13 ($3^+/2^+$)			−1.49 ($2^+/1^+$)	−1.67 ($1^+/0$)	2.61
$[Ru(tmb)_3](PF_6)_2$[a]	1.04 ($3^+/2^+$)			−1.60 ($2^+/1^+$)	−1.80 ($1^+/0$)	2.64
1	1.24 ($3^+/2^+$)			−1.39 ($2^+/1^+$)	−1.60 ($1^+/0$)	2.62
2	1.01 ($3^+/2^+$)			−1.53 ($2^+/1^+$)	*b*	2.53
3	1.23 ($5^+/4^+$)	−0.46 ($4^+/3^+$)	−0.87 ($3^+/2^+$)	−1.41 ($2^+/1^+$)	−1.61 ($1^+/0$)	
4	1.05 ($5^+/4^+$)	−0.49 ($4^+/3^+$)	−0.85 ($3^+/2^+$)	−1.46 ($2^+/1^+$)	*b*	

[a] Electrochemical data for $[Ru(tmb)_3](PF_6)_2$ was reported by Anderson et al.[105] [b] This reduction wave was not observed because of solvent reduction.

available for the parent or model complexes. This initial observation is evidence that photoinduced electron transfer is operative in **3** and **4** at rates substantially larger than $k_o \sim 1 \times 10^6\ s^{-1}$.

The featureless emission spectra of the parent and donor complexes in room temperature acetonitrile can be fit using a standard Franck−Condon analysis developed by Meyer's group and summarized by eq. 2 shown in the Experimental Section.[84–86] The results from the fitting are summarized in Table 2. For the purposes of this electron transfer study, the most important factors extracted from this analysis are E_0 and $\Delta\bar{\nu}_{0,1/2}$. E_0 refers to the energy separation between the emissive ^{3}MLCT state and the ground state to which the transition is taking place while $\Delta\bar{\nu}_{0,1/2}$ refers to the homogeneously broadened linewidth of the zeroth vibronic transition (i.e. $\nu' = 0 \rightarrow \nu'' = 0$). With this information the free energy available in the ^{3}MLCT state for these complexes, ΔG°_{MLCT} (commonly written as E_{00}), can then be calculated according to eq. 3.[87,101]

$$\Delta G^\circ_{MLCT} = E_0 + \frac{(\Delta\bar{\nu}_{0,1/2})^2}{16k_BT\ln 2} \quad (3)$$

From a photophysical point of view, the fitting results are consistent with the emission observations discussed above. Namely, both E_0 as well as the related ΔG°_{MLCT} reflect less stored excited-state energy for complex **2** in comparison to **1** or the parent species.

In terms of the photoinduced electron transfer at the heart of these studies, the ΔG°_{MLCT} determined for **1** and **2** is used to estimate the free energy available in the ^{3}MLCT excited state of **3** and **4**, respectively, for participation in charge-separation photochemistry. We were initially concerned that charge differences (+2 in the models versus +4 in the D-B-A systems) and related solvation properties would preclude using **1** and **2** to quantitatively estimate ΔG°_{MLCT} for **3** and **4**, respectively. However, as discussed above, the attachment of the doubly charged acceptor moiety through a methylene spacer has little to no effect on the energy or shape of the MLCT absorption band of the complexes (Figure 1 and Supporting Information, Figure S1a). We interpret this as evidence that the doubly charged acceptor moiety does little to perturb the ^{3}MLCT energy as well.

The lifetime of the ^{3}MLCT state in **1** and **2** was measured to establish an estimate of k_o ($1/\tau_{obs}$) for **3** and **4**, respectively. The quantity k_o refers to the rate constant of ground state recovery in the absence of electron transfer (i.e., the sum of radiative rate constants k_r and non-radiative rate constants k_{nr}). As seen in Table 1 both model complexes have similar lifetimes, with **2** being slightly shorter than **1**. Considering values obtained for E_0 (Table 2), this observation is consistent with the energy gap law.[84,102–104]

Electrochemistry. The electrochemical properties of the complexes were measured using cyclic voltammetry (CV) and are reported in Table 3. All three tmb containing complexes ($[Ru(tmb)_3]^{2+}$, **2**, and **4**) show a ~200 mV shift to lower potentials for oxidation of the metal center with respect to the bpy containing complexes. This shift is due to the stronger electron donating character of the tmb ligand as compared to bpy which stabilizes the "hole" in the oxidized Ru^{III} center. Along similar lines, $[Ru(bpy)_3](PF_6)_2$ is oxidized ($3^+/2^+$) at a potential ~100 mV less than compounds **1** or **3**. This is evidence that the aryl-substituted ligands *p*-tol-bpy or bpy-ϕ-MV^{2+} are electron withdrawing by comparison to bpy.

The electron withdrawing properties of *p*-tol-bpy (in **1** and **2**) or bpy-ϕ-MV^{2+} (in **3** and **4**) poises these aryl-substituted ligands to be the first reduced ($2^+/1^+$) in each of the bis-heteroleptic species **1**−**4**. We observe 70−140 mV shifts to lower reduction potential for each complex in comparison to its respective parent complex $[Ru(bpy)_3](PF_6)_2$ or $[Ru(tmb)_3](PF_6)_2$.

Despite the common ligand and common assignment for the first reduction wave, we note that **2** is more difficult to reduce by ~140 mV as compared to **1**. Here it is expected

(101) Chen, P.; Meyer, T. J. *Chem. Rev.* **1998**, *98* (4), 1439–1477.
(102) Robinson, G. W.; Frosch, R. P. *J. Chem. Phys.* **1963**, *38* (5), 1187–1203.
(103) Siebrand, W. *J. Chem. Phys.* **1967**, *47* (7), 2411–2422.
(104) Caspar, J. V.; Meyer, T. J. *J. Phys. Chem.* **1983**, *87* (6), 952–957.
(105) Anderson, P. A.; Anderson, R. F.; Furue, M.; Junk, P. C.; Keene, F. R.; Patterson, B. T.; Yeomans, B. D. *Inorg. Chem.* **2000**, *39* (13), 2721–2728.

that the electron donating effect of the tmb ligands in $[Ru(tmb)_2(p\text{-tol-bpy})]^{2+}$ enhances backbonding from the ruthenium to the *p*-tol-bpy ligand via a π-inductive effect when compared to $[Ru(bpy)_2(p\text{-tol-bpy})]^{2+}$.

Looking at the electrochemical data for **2** compared to **1** we see that redox perturbations attributed to the tmb ligand are smaller for the $2^+/1^+$ couple (first reduction) as compared to the $3^+/2^+$ couple (oxidation of the metal center).[106] This results in a $\Delta E_{1/2}$ (voltage difference between the oxidized and reduced forms) that is approximately 100 mV less in **2** than it is in **1**. Lever and co-workers have shown an excellent correlation between $\Delta E_{1/2}$ and E_0 for a wide variety of Ru(II) polypyridyl systems.[107] In this context, substitution of the ligand tmb for bpy in **2** versus **1** results in a smaller amount of stored excited-state energy. This is somewhat counterintuitive as one tends to think that electron-donating ligands will manifest in larger MLCT energies. The electrochemical result is consistent with the observation in a red-shifted emission band for **2** versus **1**.

The substitution of the ancillary ligand tmb for bpy (and vice-versa) has been used by Nocera and co-workers as a means of preparing MLCT excited states with specific (and functional) charge transfer direction in salt-bridged donor-acceptor systems.[108–110] In our complexes, the electrochemical and photophysical properties just discussed suggest that the asymmetric aryl-substituted ligand is the lowest energy ligand not only in the tmb-containing species **2** and **4** but also in the bpy-containing species **1** and **3**. Thus we expect the direction of the ^{3}MLCT excited state to be the same, involving formal reduction of the asymmetric aryl-substituted ligand, for each of the systems **1**−**4**. This will be important in our discussion of electron transfer (vide infra). Nocera and co-workers have observed electron transfer rates from a photoexcited Ru^{II} donor to a salt-bridged dinitrobenzoate acceptor that are slower than expected because of MLCT population of ancillary bpy ligands.[108–110] As will be discussed for **3**, we observe a forward electron transfer rate that, if anything, is larger than expected given its driving force as compared to **4**. This is consistent with the ^{3}MLCT residing on the aryl-substituted ligand which comprises the bridge in both D-B-A species.

The oxidation and reduction potentials of the donor-acceptor complexes **3** and **4** allow for the calculation of the free energy of formation of the ion-pair state according to the formulation of Weller, shown below as eq. 4.[47] The electrochemical work term from Weller's original formulation is not shown here as our electron-transfer rate constant and redox potentials were measured in the same solvent.

$$\Delta G^\circ_{IP}\,(\text{eV}) = E_{ox} - E_{red} - \frac{e^2}{4\pi\varepsilon_o\varepsilon_s R_{DA}} \times 6.242 \times 10^{18}\,\frac{\text{eV}}{J} \tag{4}$$

In this expression E_{ox} and E_{red} refer, respectively, to the $5^+/4^+$ and $4^+/3^+$ half-wave potentials of **3** and **4** from Table 3, *e* is the fundamental charge, ε_o is the permittivity of free space, ε_s is the static dielectric constant of the solvent in which the electron-transfer rate constants were measured, and R_{DA} is an estimate of the donor-to-acceptor distance[111] (values listed in Table 4). In this eq. 4, the final term corresponding to the work of separating charge in a dielectric continuum makes a relatively small contribution (<4%) to ΔG°_{IP} because the ion pair state is formed in the polar solvent acetonitrile (ε_s = 36.2). According to eqs. 5a and 5b, the quantity ΔG°_{IP} is used to calculate the driving force for both forward and reverse electron transfer in our D-B-A systems **3** and **4**. In the expression ΔG°_{MLCT} is the quantity defined in eq. 3 and listed in Table 2.

$$\Delta G^\circ_{ET} = -\Delta G^\circ_{MLCT} + \Delta G^\circ_{IP} \tag{5a}$$

$$\Delta G^\circ_{BET} = -\Delta G^\circ_{IP} \tag{5b}$$

Values for ΔG°_{ET} and ΔG°_{BET} for D-B-A complex **3** are −0.52 eV and −1.7 eV, respectively. For **4**, ΔG°_{ET} and ΔG°_{BET} are −0.62 eV and −1.5 eV, respectively. These values are also listed later in Table 4. In the comparison of electron transfer driving forces between **3** and **4** it is seen that substitution of the ligand bpy with tmb leads only to a minor (∼100 meV) increase in the exothermicity of the forward reaction. This is a result of opposing trends; namely, an easier oxidation step for the tmb-containing **4** versus **3** concomitant with storage of less excited-state energy in the ^{3}MLCT state (vide supra). These factors also manifest themselves in a smaller drop in the exothermicity (∼160 meV) of the reverse reaction for the tmb-containing **4** versus **3**.

Spectroelectrochemistry. Complexes **1**−**4** were also studied by spectroelectrochemical methods using a home-built OTTLE cell with a transparent platinum mesh working electrode. We were primarily interested in observing new visible absorption features in the D-B-A species **3** and **4** upon 1-electron reduction to be used as spectroscopic markers heralding photoinduced electron transfer. As seen in Table 3, the first reduction ($4^+/3^+$) for these two species is nearly a volt less negative than the first reduction of the respective model complexes **1** and **2**. This is commensurate with the acceptor moiety (MV^{2+}) being reduced at these lower negative potentials.[19] For compounds **1** and **2**, we observed no change in the visible absorption spectrum when holding the working electrode at 0.8 V relative to the reference

(106) The oxidation of (2) is mitigated directly by the electron donating properties of the ancillary tmb ligands. The reduction of the low energy ligand p-tol-bpy is also influenced by the ancillary tmb ligands (as discussed); however, this occurs more indirectly via back-bonding from the metal center.

(107) Lever, A. B. P. *Inorg. Chem.* **1990**, *29* (6), 1271–1285.

(108) Roberts, J. A.; Kirby, J. P.; Nocera, D. G. *J. Am. Chem. Soc.* **1995**, *117* (30), 8051–8052.

(109) Kirby, J. P.; Roberts, J. A.; Nocera, D. G. *J. Am. Chem. Soc.* **1997**, *119* (39), 9230–9236.

(110) Roberts, J. A.; Kirby, J. P.; Wall, S. T.; Nocera, D. G. *Inorg. Chim. Acta* **1997**, *263* (1−2), 395–405.

(111) This distance is a through-space measurement from the Ru(II) center to the 4,4′-carbon bond in the methyl viologen acceptor. It was estimated using an MM3 optimized structure from the HyperChem software package for both complexes (3) and (4).

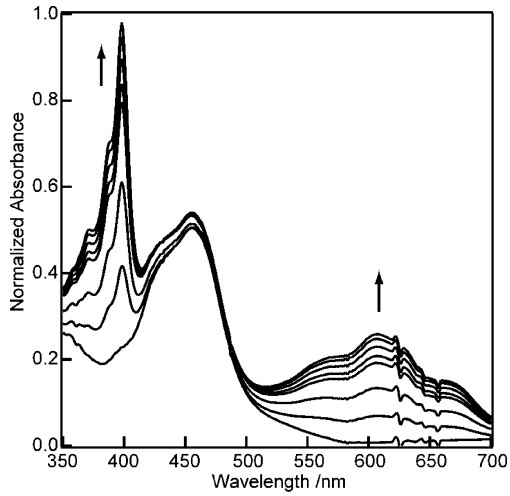

Figure 2. Spectroelectrochemical data for **3** recorded over a 15 min period of bulk electrolysis with voltage held constant at −800 mV versus Ag/$AgNO_3$. The growth of features at 375 nm and 607 nm indicate production of reduced methyl viologen. Discontinuities at 624 nm and 657 nm are an artifact of the spectrometer and how it is blanked.

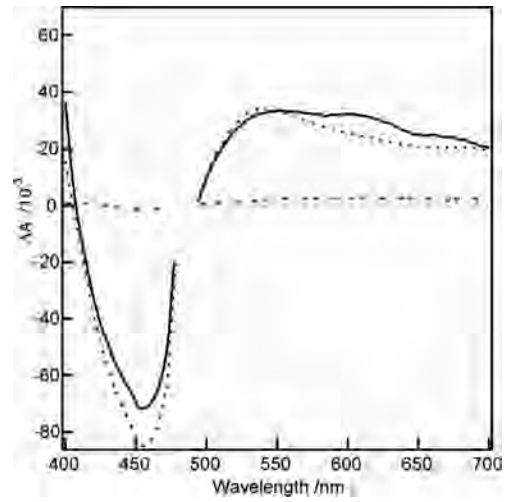

Figure 3. Transient absorption spectra for **3** in room temperature acetonitrile collected at −10 ps (dotted line), 10 ps (dashed line), 50 ps (solid line), and 750 ps (dash-dot line) following excitation with a 480 nm, ∼100 fs pump laser pulse. Data between 470 and 500 has been removed as it is strongly contaminated by scatter from the pump laser.

electrode ($Ag/AgNO_3$). In the context of Table 3, this relative voltage is equivalent to 0.5 V versus SCE. This is the expected outcome as both compounds remain in their starting redox state. For compounds **3** and **4**, this same potential leads to bulk electrolysis as the acceptor moiety on each is reduced. Figure 2 shows absorption spectra collected for **3** during 15 min of bulk electrolysis. A similar spectrum is reported for **4** in the Supporting Information, Figure S2. For both complexes we observe the growth of an intense and broad absorption feature peaked at 607 nm as the compounds change visibly from orange to green. This electronic absorption band is a well-known property of reduced methyl viologen.[112]

Transient Absorption. Transient absorption difference spectra were collected for complexes **3** and **4** with ∼1 ps time resolution dictated by the chirp[113] of our white-light probe pulses. Figure 3 and Supporting Information, Figure S3 show three such spectra for **3** and **4**, respectively, collected at $\Delta t = -10$, 10, 50, and 750 ps, where Δt refers to the arrival time in the sample of the broad-band probe pulse with respect to the ∼60 fs 480 nm excitation (pump) pulse. At early times following excitation (10 ps), the difference spectrum shows the character of the MLCT excited state; namely, an intense bleach feature centered at 452 nm concomitant with absorption features to the red. This difference spectrum is similar to that observed for related compounds such as $[Ru(dpb)_3]^{2+}$ at times ranging from 1 ps to hundreds of ns.[54,56] On the basis of previous assignments for $[Ru(dpb)_3]^{2+}$ as well as spectroelectrochemical measurements we have made for **1** upon 1-electron reduction (1.60 V vs SCE), we assign the broad absorptive feature peaked at ∼540 nm as being due to $\pi^* \leftarrow \pi^*$ transitions of the aryl-containing ligand formally reduced in the ^{3}MLCT state. The featureless absorption to the red of this (600−700 nm) is expected to arise from LMCT (ligand-to-metal charge transfer) transitions from the neutral (ancillary) ligands to the formally oxidized metal center.[56]

At later times following excitation ($\Delta t = 50$ ps), the transient difference spectrum exhibits changes indicative of the formation of the electron transfer photoproduct. Most importantly, we observe enhanced excited-state absorption at $\lambda_{probe} = 607$ nm consistent with the spectral feature uncovered by spectroelectrochemical data heralding the reduction of the acceptor moiety MV^{2+} (Figure 2). At much longer probe delay times ($\Delta t = 750$ ps), all features in the difference spectrum have decayed to very near the baseline consistent with ground-state recovery. This is occurring several orders of magnitude faster in **3** and **4** than it does in the model complexes **1** and **2** where excited-state lifetimes have been measured to be 940 ns and 870 ns, respectively (vide supra). Clearly there are additional reactive pathways for the ^{3}MLCT excited states of **3** and **4** absent in **1** and **2**. That we can observe a transient absorption at 607 nm characteristic of the charge-separated photoproduct suggests that electron transfer from the ^{3}MLCT state to the acceptor moiety (D^*-B-A→ D^+-B-A^-) is occurring.

To interrogate the proposed mechanism for excited-state evolution in the complexes **3** and **4**, we have studied wavelength-dependent kinetics with much finer Δt steps between pump and probe. Kinetics data extending to $\Delta t =$ 1 ns were collected for **3** and **4** with $\lambda_{probe} = 440$ nm, 594 nm, and 607 nm. These data are shown in Figure 4 for **3** and Figure 5 for **4** along with fits to a kinetic model as described below.

We plot these kinetics in terms of a normalized negative change in transmittance ($-\Delta T$) of the probe signal. This may be interpreted in the same way as a ΔA signal where positive features correspond to net transient absorption and negative signals correspond to net transient bleach. The wavelengths were chosen to interrogate three different regions of the transient difference spectrum and serve primarily to test the generality of our kinetics model discussed below. In all cases,

(112) Watanabe, T.; Honda, K. *J. Phys. Chem.* **1982**, *86* (14), 2617–2619.
(113) Klimov, V. I.; McBranch, D. W. *Opt. Lett.* **1998**, *23* (4), 277–279.

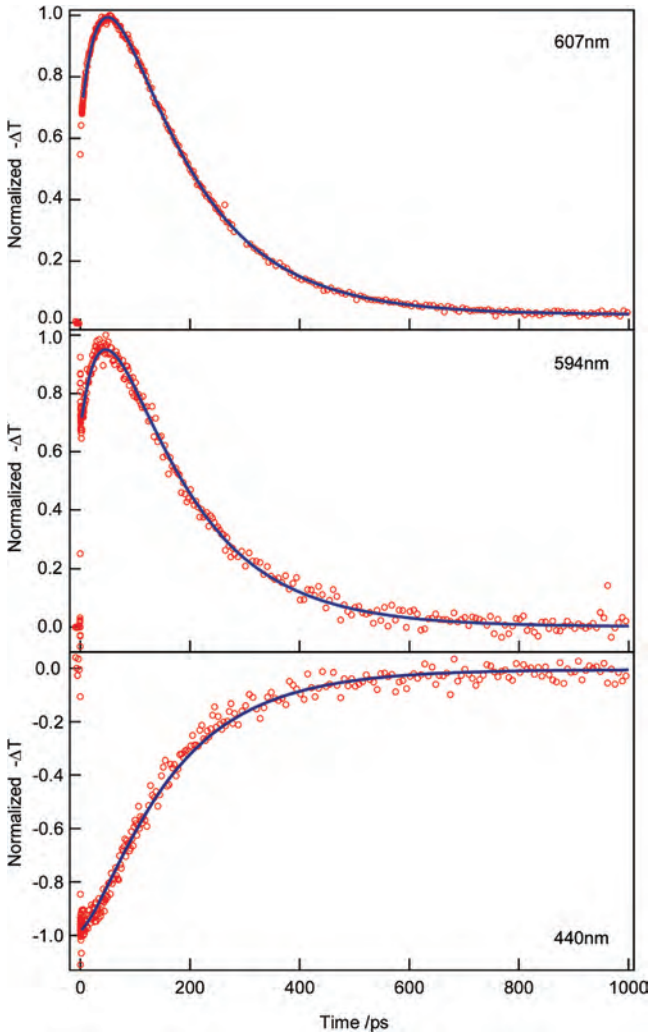

Figure 4. Transient absorption kinetics for **3** in room temperature acetonitrile collected at a probe wavelength of 607 nm (top), 594 nm (middle), and 440 nm (bottom). The raw data (circles) were fit with the kinetic model eq. 6 (solid, see text for details).

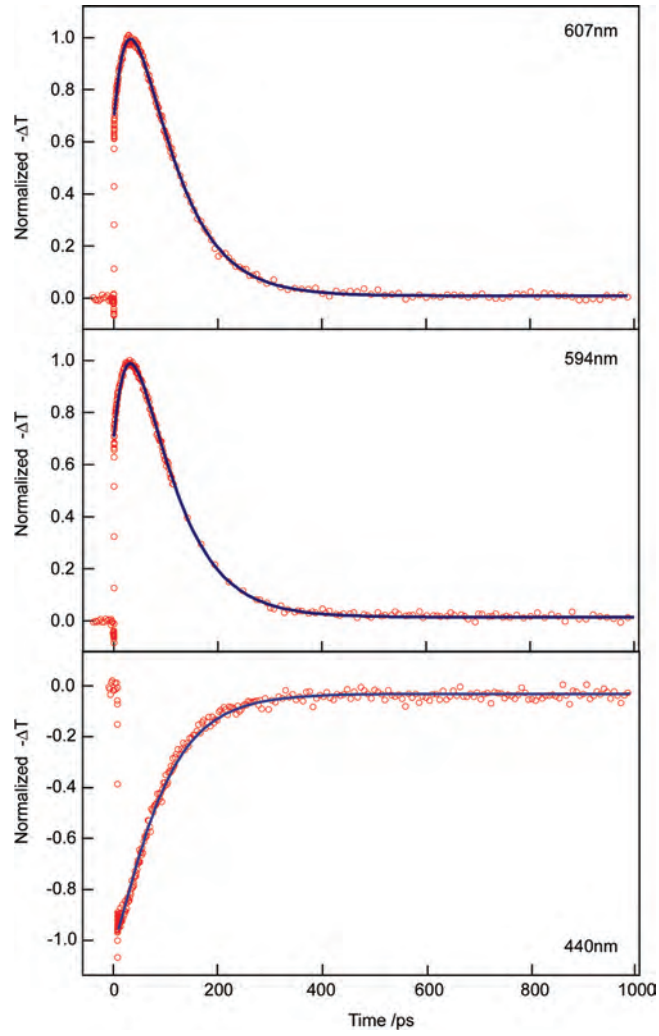

Figure 5. Transient absorption kinetics for **4** in room temperature acetonitrile collected at a probe wavelength of 607 nm (top), 594 nm (middle), and 440 nm (bottom). The raw data (circles) were fit with the kinetic model eq. 6 (solid, see text for details). The 607 nm and 594 nm data were collected under the ground-state absorption conditions, shown in the Supporting Information, Figure S1a, where there is very little colored impurity detected. The 440 nm data were collected under the ground-state absorption conditions shown in the Supporting Information, Figure S1b where a small shoulder due to a colored impurity is seen. We do not believe this impurity alters the kinetics other than in adding a small time-independent shelf (see ref 114).

the kinetics do not start from a zero background because the Franck−Condon state (^{1}MLCT) as well as the ^{3}MLCT state of either complex **3** or **4** (very close to $\Delta t = 0$ with the time steps used in these kinetics traces) have appreciable transient absorption or bleach at these wavelengths.

A general kinetics model shown as eq. 6 is based on the three-state picture shown in the Supporting Information, Scheme S1.

$$Y = Ae^{-k_{ET}t} + B\frac{k_{ET}}{k_{BET} - k_{ET}}(e^{-k_{ET}t} - e^{-k_{BET}t}) - C\left(\frac{k_{BET}}{k_{BET} - k_{ET}}e^{-k_{ET}t} - \frac{k_{ET}}{k_{BET} - k_{ET}}e^{-k_{BET}t}\right) + y_0 \quad (6)$$

This expression is readily derived for a transient signal collected as a change in absorbance where, $Y = \Delta A$. Provided that the concentration of excited-state state species remains small, which is certainly the case under our excitation conditions, it is a good approximation to expect $Y = -\Delta T$ as well. In this expression k_{ET} refers to the forward electron transfer rate constant (D*-B-A → D$^+$-B-A$^-$) while k_{BET} refers to the back electron transfer rate constant repopulating the ground state (D$^+$-B-A$^-$ → D-B-A). The quantities *A, B,* and *C* are proportional (with the same proportionality constant) to the molar extinction coefficient of the excited-state donor (D*-B-A), the electron transfer photoproduct (D$^+$-B-A$^-$), and the ground-state species (D-B-A), respectively, at the probe wavelength. The quantity y_0 is a time-independent offset needed to model our data. In this expression, we assume that relaxation via non-radiative and radiative pathways from D*-B-A directly to the ground state D-B-A can be neglected. In essence k_o (where, $k_o = k_r + k_{nr}$) is much smaller than either k_{ET} or k_{BET}. As seen in Table 1 and Table 4, this assumption is a good one because k_o is on the order of 10^6 s^{-1}, whereas k_{ET} or k_{BET} are on the order of 10^{10} s^{-1} (shown below). We also neglect a rate constant (k_{rev}) involving the repopulation of the ^{3}MLCT from D$^+$−B−A$^-$. With forward reaction free energies ($\Delta G°_{ET}$) on the order of −0.5 eV (see

Table 4), the equilibrium constant for the electron transfer process is very large (on the order of 10^8) and we can ignore k_{rev}.

We have fit the data collected for both **3** and **4** at $\lambda_{probe} = 607$ nm using eq. 6 with all free parameters with the exception of the quantity C which has been fixed at $C = 0$ because the ground states of these molecules do not absorb at this probe wavelength. We have done this for three separate data sets collected for both **3** and **4** at $\lambda_{probe} = 607$ nm. The signal-to-noise of the data shown in the top panels of Figures 4 and 5 is representative of each of the separate measurements. The quality of the fit (solid line) in both figures is also representative of the separate measurements. In the Supporting Information we report the fitting parameters that have been determined for these two molecules (Supporting Information, Table S1). We note here that the time independent offset y_0 needed to model our data is a very minor contributor to the data as a whole. As seen in Supporting Information, Table S1 for **3**, the quantity y_0 is ~5% of the quantity A and ~2% of the quantity B. For compound **4**, y_0 is ~3% of the quantity A and ~1% of the quantity B.[114]

It is important to note that eq. 6 can be used to model the data in two different ways with equal quality in the least squares fitting. In the first case, $k_{ET} > k_{BET}$ and we can interpret the kinetics at $\lambda_{probe} = 607$ nm in an intuitive way where the rise and decay features of the data reflect the production and subsequent loss of the electron transfer photoproduct with rate constants of k_{ET} and k_{BET}, respectively.

In the second case, $k_{BET} > k_{ET}$, a condition that has been called inverted kinetics.[115] The fits of the $\lambda_{probe} = 607$ nm data for both **3** and **4** according to this scenario reveal the expected result that the parameter B is changed, the parameter A remains the same, and the values of k_{BET} and k_{ET} simply switch with respect to the first case discussed above where $k_{ET} > k_{BET}$. While less intuitive, this scenario is nonetheless possible and the validity of either the first case ($k_{ET} > k_{BET}$) or the second case ($k_{BET} > k_{ET}$) must be explored with additional measurements/information.

The most straightforward way to explore the validity of either model $k_{ET} > k_{BET}$ or $k_{BET} > k_{ET}$ is to obtain an independent measurement of k_{ET} from time-resolved emission experiments. Unfortunately, this is very difficult for these systems. The radiative rate constants for **3** and **4** from the ^{3}MLCT state would be expected to be small and on the order of 10^5 based on comparisons to the model complexes **1** and **2** (see Table 1). As such, very few photons would be emitted on the time scale of the electron transfer event. For example, of the total number of photons emitted by the ^{3}MLCT state of **1** and **2**, only ~0.01% come in the first 100 ps. A second possibility is to identify an absorptive spectral feature of the excited state in **3** and **4** that is dominated by the photoexcited donor (D*-B-A), thereby isolating the first term in eq. 6. Again, this is unfortunately not possible for these systems given our experimental configuration for visible transient absorption. This can be seen in the spectroelectrochemistry data reported in Figure 2 and Supporting Information, Figure S2 for **3** and **4**, respectively. These data show that either reduced methyl viologen *or* the molecular ground state is strongly absorptive in all regions of the UV-vis spectrum within which we might be able to probe excited states (400−700 nm). In other words, there are no spectral regions where absorptive features of D*-B-A will dominate.

Table 4. Electron Transfer Data of Complexes in Room Temperature CH_3CN[a]

complex	**3**	**4**
$\Delta G°_{ET}$/eV	−0.52	−0.62
$\Delta G°_{BET}$/eV	−1.7	−1.5
$k_{ET}/10^{10}$ s^{-1}	2.6 ± 0.1	2.8 ± 0.02
$k_{BET}/10^{10}$ s^{-1}	0.62 ± 0.04	1.37 ± 0.06
τ_{ET}/ps	38	36
τ_{BET}/ps	160	73
R_{DA}	13.6	13.8

[a] The error bars reported in this table represent 2σ determined from fitting three separate measurements of kinetics collected at $\lambda_{probe} = 607$ nm for each complex.

In principle it should be possible to use the values of the fitting parameters A and B ($C = 0$ at $\lambda_{probe} = 607$ nm) to validate $k_{ET} > k_{BET}$ or $k_{BET} > k_{ET}$. However, this analysis requires knowledge of the extinction coefficients for D^+-B-A^- and D*-B-A at $\lambda_{probe} = 607$ nm. At this time we do not know these quantities with sufficient certainty to argue unambiguously for either model. A simplified analysis is presented in the Supporting Information. The results argue strongly in favor of the assignment $k_{ET} > k_{BET}$ for **4**. For **3**, the results are more ambiguous but at the same time do not argue against the assignment $k_{ET} > k_{BET}$.

Despite the difficulties encountered in validating $k_{ET} > k_{BET}$ or $k_{BET} > k_{ET}$, our interpretation of the electron transfer phenomena in these systems **3** and **4** made throughout the rest of this manuscript strongly favors the case where $k_{ET} > k_{BET}$. Thus, in Table 4 we present the results of our kinetics analysis according to this model along with the electron transfer reaction free energies discussed previously.

These data suggest that the conformational flexibility of the bridge separating D and A in **3** and **4** is not large enough to provide a route towards energy-wasting charge-recombination (ground-state recovery via back electron transfer) at a rate larger than forward electron transfer. This is the expected result if we consider that the main source of conformational flexibility that would alter the distance between D^+ and A^- is the methylene spacer and not the aryl-substituent. In earlier work on D-B-A systems linking Ru(II) MLCT excited-state donors with MV^{2+} acceptors, Mallouk, Schmehl, and co-workers consistently observed $k_{ET} > k_{BET}$ when a methylene spacer separated D and A even as they altered driving-force properties through substituent changes to the metal complex and the acceptor.[48] This is not true if ethyl or larger carbon chains are used to separate the MLCT excited state donor from a methyl viologen moiety or a similar di-quaternary ammonium (diquat) acceptor.[89,91–93]

(114) We also note that when we model kinetics collected for (4) under visible absorption spectrum circumstances shown in Supporting Information, Figure S1(b) where a minor MLCT shoulder is observed because of an impurity, we obtain essentially identical values for k_{ET} and k_{BET} to those reported in Table 4. Under these circumstances the offset y_o is slightly larger and is 9% of A and 4% of B.

(115) Palacios, R. E.; Kodis, G.; Gould, S. L.; Garza, L. d. l.; Brune, A.; Gust, D.; Moore, T. A.; Moore, A. L. *ChemPhysChem* **2005**, *6* (11), 2359–2370.

Hammarstrom and co-workers have also recently observed $k_{ET} > k_{BET}$ for a D-B-A system linking a methyl viologen moiety to a Ru^{II} polypyridyl excited state donor through a methylene spacer.[90]

To model the kinetics data at $\lambda_{probe} = 594$ nm and 440 nm for **3** and **4**, we used fixed values of k_{ET} and k_{BET} obtained from the free-parameter fits of the $\lambda_{probe} = 607$ nm data discussed above. As seen in Figures 4 and 5, the fits to the $\lambda_{probe} = 594$ nm and 440 nm data with fixed values of k_{ET} and k_{BET} are quite reasonable. The kinetics at $\lambda_{probe} = 594$ nm are, as expected, similar to the $\lambda_{probe} = 607$ nm data with a slightly larger contribution because of the MLCT state in comparison to the absorbance of the reduced methyl viologen (Supporting Information, Table S1). For the $\lambda_{probe} = 440$ nm data, the inflection of the transient bleach dynamics collected at early times (Figures 4 (bottom) and 5 (bottom)) arises because both the D*-B-A species formed at early times as well as the D^+-B-A^- species formed with k_{ET} should be substantially less absorptive than the ground state. This means that the bleach should recover in a delayed fashion dependent on k_{BET}. The "spike" at $\sim\Delta t = 0$ in kinetics data for **3** and **4** have not been considered in our model.[116]

A comparison of electron transfer rates between **3** and **4** shows interesting properties. The forward rates k_{ET} are quite similar, whereas the reverse rates k_{BET} are different by approximately a factor of two. Initially we considered the observation concerning k_{BET} to be unusual; however, semiclassical electron transfer theory adequately predicts these rate differences based on the change in the driving force (ΔG°_{BET}) between these two compounds, that is, where these reactions are taking place within the Marcus inverted region. The equation used to model the rate differences (k_{BET}) between **3** and **4** as a function of ΔG°_{BET} is shown here as eq. 7.[117–120]

$$k_{BET} = \sqrt{\frac{4\pi^3}{h^2\lambda_{low}k_BT}}|H_{ab}|^2\sum_n e^{-S}\frac{S^n}{n!}\times \exp\left[\frac{-(\Delta G^\circ_{BET}+\lambda_{low}+n\hbar\omega)^2}{4\lambda_{low}k_BT}\right] \quad (7)$$

In this expression, ω refers to the angular frequency of the single (average) quantum mechanical promoting vibrational mode, the index n runs over the number of these modes ($\hbar\omega$) needed to describe Franck−Condon overlap between the D^+-B-A^- state and the D-B-A ground state, and S refers to the Huang−Rhys factor ($S = \lambda_i/\hbar\omega$) where λ_i is the intramolecular reorganization energy. The quantity λ_{low} refers to the solvent reorganization energy which can be predicted by the Marcus two-sphere continuum model as shown here in eq. 8.[121,122]

$$\lambda_{low}(J) = \frac{e^2}{4\pi\varepsilon_0}\left(\frac{1}{2R_D}+\frac{1}{2R_A}-\frac{1}{2R_{DA}}\right)\left(\frac{1}{\varepsilon_\infty}-\frac{1}{\varepsilon_s}\right) \quad (8)$$

In this expression, e is the fundamental charge being transferred, ε_0 is the permittivity of free space, R_D and R_A are the radii of the donor and acceptor moieties, respectively, R_{DA} is the through-space center-to-center distance between donor and acceptor,[111] and ε_∞ and ε_0 are the high-frequency and static dielectric constants of the solvent, respectively.

At this stage of our research we do not know values for H_{ab} and do not have sufficient k_{BET} rate constants to obtain it with a fit of driving-force dependence data to eq. 7. Nonetheless, we can use literature precedent as a starting place for $\hbar\omega$, S, and λ_{low} and then vary H_{ab} to approximate our data. For similar systems (absent the phenylene spacer but containing the methylene spacer) Mallouk and co-workers have modeled the inverted region electron transfer data with $\hbar\omega = 1100$ cm^{-1} and $S = 3$. These workers have shown that care must be taken in quantifying the radius of the reduced methyl viologen acting as a donor because of its ellipsoidal (halibut) shape.[89] They empirically find a 4.8 Å sphere for the donor to be in the best agreement to their ellipsoidal model. If we use this number, a 6.8 Å sphere for the $Ru^{III}(L)_3$ acceptor moiety,[89] and a 13.7 Å value for R_{DA} based on molecular mechanics minimization calculations of **3** and **4** (vide supra), eq 8 predicts $\lambda_{low} = 0.80$ eV. Now setting $\lambda_{low} = 0.80$ eV, $\hbar\omega = 1100$ cm^{-1}, $S = 3$, and $H_{ab} = 10.96$ cm^{-1}, eq 7 predicts a time constant for back electron transfer of 160 ps when $\Delta G^\circ_{BET} = -1.7$ eV (i.e., for **3**) and 74 ps when $\Delta G^\circ_{BET} = -1.5$ eV (i.e., for **4**). This is in excellent agreement with our data. This further substantiates our conclusion that the kinetics data for **3** and **4** are correctly interpreted under the scenario where $k_{ET} > k_{BET}$.[123]

It should be emphasized that there are too many parameters within eq. 7 to trust our modeled values of H_{ab} with a great

(116) These reflect ultrafast dynamics complete within 200 fs—presumably because of the ^{1}MLCT and ^{3}MLCT of D*-B-A—convolved with coherence signals present when the pump and the probe are temporally overlapped in the sample.

(117) Jortner, J. *J. Chem. Phys.* **1976**, *64* (12), 4860–4867.

(118) Fischer, S. F.; Vanduyne, R. P. *Chem. Phys.* **1977**, *26* (1), 9–16.

(119) Hopfield, J. J. *Proc. Natl. Acad. Sci. U.S.A.* **1974**, *71* (9), 3640–3644.

(120) DeVault, D. *Quantum Mechanical Tunneling in Biological Systems*; Cambridge University Press: Cambridge, 1984.

(121) Marcus, R. A. *J. Chem. Phys.* **1956**, *24* (5), 966–978.

(122) Marcus, R. A. *Annu. Rev. Phys. Chem.* **1964**, *15*, 155–196.

(123) We can further argue that our assignment that $k_{ET} > k_{BET}$ is correct based on discussions of solvent reorganization energies. If the opposite were true, that is, if $k_{BET} > k_{ET}$, we would need to rationalize why back electron transfer rate constants for (**3**) and (**4**) would be nearly identical despite a 200 meV difference in between the two compounds. This would require near-barrierless back electron transfer reactivity for the two compounds with (**3**) slightly in the normal region and (**4**) slightly in the inverted region of a Marcus parabola based on eq 7. Assuming the two compounds have the same internal reorganization energy for back electron transfer ($\lambda_i = 3300$ cm^{-1}; see text for details)—an assumption based on nearly identical electron transfer distance and expected similarities in the electronic structure of both D^+-B-A^- and D-B-A between the two compounds—a solvent reorganization energy of $\lambda_{low} = 1.19$ eV is needed to reproduce the appropriate ratio of rate constants $k_{ET(3)}/k_{ET(4)} = 0.93$. To our knowledge, a solvent reorganization energy of this size has no precedence in the literature for similar electron transfer systems in acetonitrile. The use of eq. 8 to calculate a solvent reorganization energy $\lambda_{low} = 1.19$ eV would require that the reduced methyl viologen acting as donor be modeled with a physically unrealistic sphere of radius 3.2 Å rather than the 4.8 Å sphere determined empirically by Mallouk and co-workers (cf. 89, see text for details).

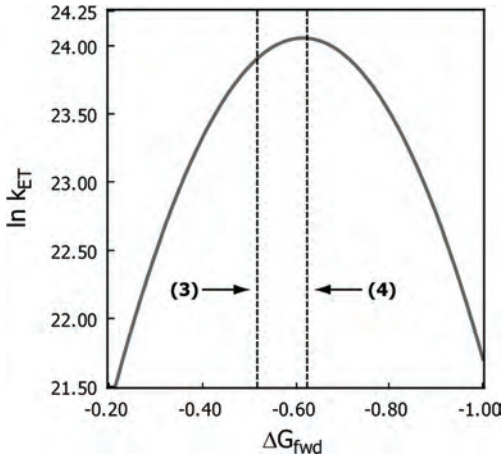

Figure 6. Prediction of the natural log of k_{ET} versus $\Delta G°_{ET}$ (see eq. 9) if $\lambda = 0.59$ eV and $H_{ab} = 9.2$ cm^{-1}. The dotted lines reflect the measured $\Delta G°_{ET}$ for compounds **3** and **4**. The choice of $\lambda = 0.59$ eV is required to match the small percentage increase in k_{ET} between **3** and **4**.

deal of certainty. Nonetheless, the order of magnitude appears correct.[124,125]

More interesting than the rate differences for back electron transfer in **3** versus **4** are the rate similarities (k_{ET}) for the forward reaction. Despite a 100 meV increase in driving force between **3** (−0.52 eV) versus **4** (−0.62 eV), the rate constant k_{ET} only increase by ∼8%. A similar increase in driving force for systems studied by Mallouk, Schmehl, and co-workers as well as Kelley, Elliot, and co-workers show rate changes of ∼60% and ∼62%, respectively.[48,92] We can coarsely model our observation of similar rate constants using the classical Marcus equation to describe the forward electron transfer rate.

$$k_{ET} = \sqrt{\frac{4\pi^3}{h^2 \lambda k_B T}} |H_{ab}|^2 \exp\left[\frac{-(\Delta G_{ET} + \lambda)^2}{4\lambda k_B T}\right] \qquad (9)$$

In this expression the reorganization energy λ contains both inner-sphere and outer-sphere contributions. If we assume that H_{ab} is the same for **3** and **4** (an assumption based on nearly identical electron transfer distance and expected similarities in the electronic structure of both D*-B-A and D^+-B-A^- between the two compounds), then the ratio of rates (k_{ET} for **3**/k_{ET} for **4**) will depend only on the value of λ. To achieve the appropriate ratio (in our case k_{ET} for **3**/k_{ET} for **4** = 0.93) the value for λ would be ∼0.59 eV. This reorganization energy suggests that the forward electron transfer reaction would be close to barrierless ($-\Delta G°_{ET} = \lambda$) for both **3** and **4**. This scenario is shown in Figure 6 where we have set $H_{ab} = 9.2$ cm^{-1} to obtain a forward electron transfer time constant of 38 ps for **3** (where $\Delta G°_{ET} = -0.52$ eV) and 36 ps for **4** (where $\Delta G°_{ET} = -0.62$ eV). It is important to stress that the comparative analysis above assumes the two complexes **3** and **4** have identical reorganization energies and identical values for H_{ab}. Additional measurements are needed to independently confirm that these systems are exhibiting near barrierless forward electron transfer. Along these lines, we will report on temperature effects on these rate constants at a later date.

At this point we do not have a good explanation why the forward and back electron transfer processes are best modeled with such similar values for H_{ab} ($H_{ab} = 9.2$ cm^{-1} for the forward direction and $H_{ab} = 10.96$ cm^{-1} for the reverse direction (vide supra)). We note that in related systems, again with a methylene spacer but absent the phenylene spacer, a larger H_{ab} has been reported for the reverse direction ($H_{ab} = 62$ cm^{-1}) than the forward direction ($H_{ab} = 24$ cm^{-1}).[89]

A value of $\lambda \sim 0.59$ eV for the forward electron transfer in **3** and **4** is quite small. Previous analyses of forward electron transfer rates in similar systems (without the phenylene spacer but containing a methylene spacer)[48,89] suggest a reorganization energy of 0.7 eV partitioned between the inter- and intra-molecular contributions ($\lambda_i = 0.2$ eV and $\lambda_o = 0.5$ eV).[89] If the distance from the bipyridine moiety (formally reduced in the MLCT excited state) to the acceptor were the only factor to consider, we would expect a reorganization energy in **3** and **4** that is larger than 0.7 eV driven primarily by increases in λ_o as predicted by eq. 8.

We believe that the small reorganization energy ($\lambda \sim 0.59$ eV) for forward photoinduced electron transfer in **3** and **4** is a consequence of excited-state electron delocalization on the aryl-substituted bipyridine following MLCT excitation of the respective chromophore. As is well known in Ru(II) polypyridyl systems, MLCT excitation is characterized by charge transfer from a metal-based formally nonbonding d-orbital of π symmetry to a ligand-based orbital of π^* symmetry. A thermalized MLCT state therefore differs from the ground state on nuclear coordinates (ΔQ) involving relative bond-distances within the pyridyl rings of the formally reduced ligand. When aryl substituents are bound to the bipyridine species with minimal steric hindrance to ring rotation, further excited-state electron delocalization can occur that takes advantage of a larger π^* system. This results in mitigated nuclear coordinate changes (ΔQ) in the excited state with respect to the ground state. In the context of model complexes **1** and **2**, such delocalization decreases S_M on high-frequency vibrational coordinates such as ring-breathing modes important for nonradiative relaxation. This effect can be seen cursorily in Table 2 and will be discussed in more detail elsewhere. In **3** and **4**, excited-state delocalization would have a related effect tied directly to the electron transfer photochemistry. Here, delocalization involving the aryl-substituent of the bipyridine ligand mitigates the difference in geometry between D*-B-A and D^+-B-A^- thereby decreasing the intramolecular reorganization energy λ_i. Nuclear coordinate changes within the acceptor would be the same but those within the donor would be smaller. Arguments can also be crafted as to why excited-state delocalization would decrease the solvent reorganization

(124) Mallouk and co-workers have reported Hab = 62 cm^{-1} for their system with a methylene spacer (cf. 89). If this number is decreased to obtain ∼10.96 cm^{-1} (i.e., 10.96 cm^{-1} = 62 cm^{-1} × $e^{-\beta R}$) where $R = 2.8$ Å is the approximate distance across a phenyl group (added in our systems (**3**) and (**4**)), one obtains $\beta = 0.62$ Å^{-1}. This value for β is close to the expected range of 0.2−0.6 Å^{-1} for an unsaturated bridge (cf. 31, 71, and 125).

(125) Ribou, A. C.; Launay, J. P.; Takahashi, K.; Nihira, T.; Tarutani, S.; Spangler, C. W. *Inorg. Chem.* **1994**, *33* (7), 1325–1329.

energy λ_o.[126,127] Thus, we expect both inner *and* outer sphere contributions to the reorganization energy λ to be mitigated by ligand-based delocalization phenomena.

Conclusions

We have been interested in designing D-B-A systems with excited-state ligand-based conformational dynamics that are favorable to achieving forward photoinduced electron transfer producing D^+-B-A^- from D^*-B-A while also hindering back electron transfer producing D-B-A from D^+-B-A^-. Ideal systems would separate charge following photon absorption with a minimal reliance on driving force $\Delta G°_{ET}$. The energy-wasting reverse reaction would be hindered by small electron coupling between D^+-B-A^- and D-B-A (made smaller by the desired conformational dynamics) as well as the placement of the reaction in the Marcus inverted region (where $-\Delta G°_{BET} > \lambda_{total}$). To begin exploring these design principles we synthesized two new D-B-A systems $[Ru(bpy)_2(bpy\text{-}\phi\text{-}MV)](PF_6)_4$ (**3**) and $[Ru(tmb)_2(bpy\text{-}\phi\text{-}MV)](PF_6)_4$ (**4**) along with respective photophysical model complexes $[Ru(bpy)_2(p\text{-}tol\text{-}bpy)](PF_6)_2$ (**1**) and $[Ru(bpy)_2(p\text{-}tol\text{-}bpy)](PF_6)_2$ (**2**). Extensive photophysical studies as well as electrochemistry on all four compounds have allowed us to assign both forward and reverse electron transfer driving forces. Substituting the more electron rich tmb peripheral ligands for the bpy peripheral ligands increases the forward driving force ($\Delta G°_{ET}$) by ~100 meV (−0.52 eV for **3** to −0.62 eV for **4**) while reducing the reverse driving force ($\Delta G°_{BET}$) by ~200 meV (−1.7 eV for **3** to −1.5 eV for **4**). For both **3** and **4** we observe the electron transfer photoproduct and can assign forward and reverse electron transfer rates.

The most striking result of these studies is the similar forward electron transfer rates (k_{ET}) measured for **3** and **4** despite the ~100 meV increase in $\Delta G°_{ET}$ between the two compounds. We can explain this effect if the reorganization energy for electron transfer in this class of D-B-A systems is relatively small (compared to other known species juxtaposing a Ru(II) polypyridyl donor with a paraquat acceptor) and similar in magnitude to the forward driving force $\Delta G°_{ET}$ such that the electron transfer reactivity is nearly without barrier. Such a diminished reorganization energy is understandable from both intermolecular and intramolecular points of view if the D* moiety of the photoexcited D*-B-A in **3** and **4** can exploit the aryl-substituent of the formally reduced lowest-energy bipyridine ligand to further delocalize electron density in a larger π^* system. Such excited-state electron delocalization is a well-documented phenomenon in other MLCT systems.[25,54–57,128–132] This analysis suggests that these new systems **3** and **4**, by virtue of substituents designed into their structures, undergo forward electron transfer at a near-maximum rate for their particular driving force $\Delta G°_{ET}$ and the choice of room-temperature acetonitrile as a solvent. Certainly, strategies for reducing the reorganization energy (λ) further by altering solvent or manipulating the acceptor structure while still exploiting electron delocalization phenomena in the photoexcited donor will allow us to store even more of the excited-state energy in the charge-separated (D^+-B-A^-) state.

The question of whether ligand-based excited state motion leads to the electron delocalization favorable for electron transfer (process (ii) in Scheme 1) can be inferred from unpublished electronic structure calculations undertaken in our laboratory that will be reported at a later date.[133] A density functional theory optimized gas-phase structure of compound **1**[134] (a model for the behavior of **3**) shows that the inter-ring dihedral angle (between the aryl substituent and bipyridine to which it is bound) is $\theta = 41°$. A geometry-optimized model[134] of the ^{3}MLCT excited state suggests the dihedral angle shrinks to $\theta = 27°$, presumably concomitant with excited-state electron delocalization.[135] Our final angle does not go to completion ($\theta = 0°$)[55] arguably because of steric effects in relative agreement with results by Baranovskii and coworkers.[59] It should be noted that the polar medium will undoubtedly be important in determining the final delocalized geometry, a point that gas-phase calculations do not address.

The second main design principle of Scheme 1, wherein reverse ring-rotation motions following forward electron transfer are useful for reducing back electron transfer rates (process (iv)), is a work in progress. Both **3** and **4** are expected to exhibit similar motions and, while the measurement of their back electron transfer rates is an important step in uncovering evidence for this type of control, additional data is needed. Our next steps in this regard involve synthesis and study of systems incorporating additional steric hindrance at positions ortho to the aryl-bpy inter-ring connection at the heart of these D-B-A systems (i.e., manipulating **R** in Scheme 1). The trick will be to allow for some excited-state electron delocalization, that which we have concluded is useful for reducing reorganization energy in the forward electron transfer direction, while turning down H_{ab} through conformational changes that alter the superexchange pathway linking D^+-B-A^- to D-B-A.

(126) It should also be pointed out that excited-state ligand-based delocalization prior to electron transfer would both increase the size of the electron donor and reduce the total distance for electron transfer in the eyes of the polar solvent. Provided that solvent relaxation about the more delocalized MLCT state occurs before electron transfer (an effect we fully expect based on previous ultrafast studies of related molecules(cf. 56, 63, 64, and 127), the solvent reorganization energy λ_o would be decreased as predicted by the Marcus two-sphere continuum model (eq 8).

(127) Monat, J. E.; McCusker, J. K. *J. Am. Chem. Soc.* **2000**, *122* (17), 4092–4097.

(128) Phifer, C. C.; McMillin, D. R. *Inorg. Chem.* **1986**, *25* (9), 1329–1333.

(129) Boyde, S.; Strouse, G. F.; Jones, W. E.; Meyer, T. J. *J. Am. Chem. Soc.* **1990**, *112*, 7395–7396.

(130) Strouse, G. F.; Schoonover, J. R.; Duesing, R.; Boyde, S.; Jones, W. E.; Meyer, T. J. *Inorg. Chem.* **1995**, *34* (2), 473–487.

(131) Treadway, J. A.; Loeb, B.; Lopez, R.; Anderson, P. A.; Keene, F. R.; Meyer, T. J. *Inorg. Chem.* **1996**, *35* (8), 2242–2246.

(132) Hammarstrom, L.; Barigelletti, F.; Flamigni, L.; Indelli, M. T.; Armaroli, N.; Calogero, G.; Guardigli, M.; Sour, A.; Collin, J. P.; Sauvage, J. P. *J. Phys. Chem. A* **1997**, *101* (48), 9061–9069.

(133) Meylemans, H.; Damrauer, N. H.,manuscript in preparation.

(134) Calculated using the ADF Density Functional Theory package with the following conditions. Exchange: Generalized Gradient Corrected Becke 88; Correlation Functional: Lee-Yang-Parr; Basis Set: TζP2P (C,N, and H) and TζP (Ru with frozen 3d core).

(135) Added at time of proof. Initial Hartree-Fock calculations show the dihedral angle of the ^{3}MLCT state to be ~1°. Further information on these results will be published in the future.

Acknowledgment. This work was supported by the University of Colorado. We thank Joshua Thomas Hewitt for assistance in collecting data for Figure 5, Professor Carl Koval for assistance and the equipment used in the electrochemical measurements, and Dr. Richard Shoemaker for assistance with the NMR experiments.

Supporting Information Available: Additional figures, a scheme with a three-state picture used to derive the kinetics model, a table with fitting details for kinetics reported for complexes, and so forth (PDF). This material is available free of charge via the Internet at http://pubs.acs.org.

IC701776K